NASA CR 114,491

AVAILABLE TO THE PUBLIC

GENERATION OF NEP HELIOCENTRIC TRAJECTORY DATA

AMA Report No. 72-43
September 1972

by

Jerry L. Horsewood and Katherine B. Brice

Prepared under Contract NAS2-6946 by
ANALYTICAL MECHANICS ASSOCIATES, INC.
Seabrook, Maryland 20801

for

AMES RESEARCH CENTER

NATIONAL AERONAUTICS AND SPACE ADMINISTRATION

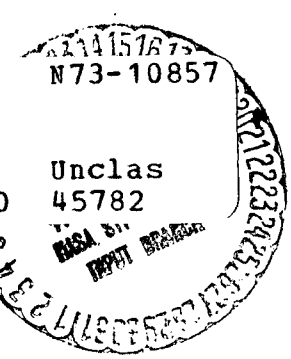

ANALYTICAL MECHANICS ASSOCIATES, INC.
10210 GREENBELT ROAD
SEABROOK, MARYLAND 20801

SUMMARY

This report details the work accomplished under NASA contract NAS2-6946, "Generation of NEP Heliocentric Trajectory Data." The principal purposes of the study were to generate representative nuclear electric propulsion data for rendezvous missions to the comet Encke using the variational calculus program HILTOP, to compare the data with equivalent data generated with the QUICKTOP program, and to propose approaches for storing and subsequently accessing the optimum trajectory and performance data in the QUICKLY program which is used for preliminary mission analysis studies.

Optimum trajectories were generated with arrival at Encke 50 days prior to perihelion passage during the 1980 apparition. Four distinct trajectory classes covering a flight time range of 400-1400 days were investigated. The data presented in this report consist of plots of the energy parameter $J = \int a^2 dt$, the propulsion time ratio t_p/t_f, and the arithmetic mean of the thrust acceleration $\bar{a} = (a_o a_f)^{\frac{1}{2}}$ as functions of the flight time for selected values of the launch excess speed in the range 0-8 km/sec. Tables of these three parameters and of the power to initial mass ratio p_o/m_o, the net spacecraft mass ratio m_n/m_o and the jet exhaust speed c are also presented. The comparison of data indicates that the HILTOP and QUICKTOP program results for the mission investigated differ only minimally with the exception of the propulsion time. The final section of this report is devoted to a discussion of suggested modifications to the computer program QUICKLY to extend its capability and improve its accuracy.

TABLE OF CONTENTS

LIST OF TABLES

LIST OF FIGURES

INTRODUCTION

In 1969, the Boeing Company, under contract to the Advanced Concepts and Missions Division (formerly Mission Analysis Division) at Moffett Field, California developed a low thrust trajectory optimization code CHEBYTOP[1]. Subsequently, ACMD personnel developed a driver package which calls CHEBY-TOP to obtain the optimum trajectory and then calculates vehicle masses and other parameters necessary for mission analysis studies. This program, known as QUICKTOP, was found to be easy to operate, relatively inexpensive to use, generally reliable in the sense of trajectory convergence and sufficiently accurate for most preliminary mission studies. In short, QUICKTOP has proved to be a useful and handy tool for low thrust mission analysis. Recently, more advanced versions of both CHEBYTOP[2] and QUICKTOP[3] were developed and are presently in widespread use.

ACMD personnel also developed another low thrust mission analysis computer program known as QUICKLY[4]. This program contains precomputed trajectory and performance data stored in polynomial form. Interpolation techniques are then used in conjunction with the characteristic length relations and other empirical formulas to estimate performance variations as a function of various propulsion system parameters. In generating data of selected missions for QUICKLY using QUICKTOP, considerable scatter, or erratic behavior, in the data was noted for certain parameters, principally the propulsion time, making the curve fitting of that data for QUICKLY particularly difficult.

The study described in this report was undertaken for the following purposes: (1) to generate optimal NEP heliocentric trajectory data using the variational calculus program HILTOP[5] for a selected mission for which substantial scatter was observed; (2) to isolate any significant discrepancies between the results obtained from QUICKTOP and those from HILTOP; and (3) to consider alternate techniques in the program QUICKLY to expand its capability, improve its accuracy, and/or extend its flexibility while reducing the volume of data that must be stored.

NOTATION

Parameter	Definition
a	semi-major axis; also, thrust acceleration
$\bar{a}$	arithmetic mean thrust acceleration
a_f	final thrust acceleration
a_o	initial thrust acceleration
b	coefficient employed in definition of efficiency factor
c	jet exhaust speed of NEP system
d	coefficient employed in definition of efficiency factor
e	eccentricity
f	thrust magnitude
h_σ	step function equal to zero if switch function is negative and equal to one if switch function is positive
i	orbital inclination relative to ecliptic plane
J	energy factor = $\int_{t_o}^{t_f} a^2 dt$
k_t	low thrust propellant tankage factor
m	spacecraft mass
m_n	net spacecraft mass
m_o	initial spacecraft mass
m_{ps}	propulsion system mass
p_b	beam power of NEP propulsion system
p_o	power into power conditioning system
$p_{o_{opt}}$	optimum power level for a spacecraft using a specified launch vehicle

Parameter	Definition
p_o^*	limiting power level below which more net mass can be achieved by off loading the launch vehicle
R	heliocentric position vector of spacecraft
r	magnitude of R
t_f	flight time
t_o	initial time or launch date
t_p	accumulated time that propulsion system has operated during the mission
v_∞	hyperbolic excess speed
α	specific propulsion system mass
η	total efficiency of the propulsion system
η'	derivative of efficiency with respect to jet exhaust speed
Λ	primer vector
λ	magnitude of Λ
λ_{ao}	multiplier adjoint to initial thrust acceleration
λ_c	multiplier adjoint to jet exhaust speed
λ_ν	multiplier adjoint to mass ratio
μ	gravitational constant of the sun
ν	instantaneous mass to initial mass ratio
ν_n	net spacecraft mass ratio
ν_p	low thrust propellant mass ratio
ν_{ps}	NEP propulsion system mass ratio
ν_t	propellant tankage mass ratio

Parameter		Definition
σ	-	engine switching function
τ	-	perihelion passage date
ω	-	argument of perihelion
Ω	-	ecliptic longitude of ascending node

DATA GENERATION

1. Study Guidelines.

The mission selected for study in this contract is the comet Encke rendezvous mission, arriving at the target 50 days prior to perihelion passage in the 1980 apparition. This corresponds to a Julian date of arrival of 2444530 (October 17, 1980). The study was restricted to the heliocentric portion of the mission with the arrival excess speed fixed at zero. Launch excess speeds in the range 0-8 km/sec were investigated for total flight times in the range 400-1400 days. A launch vehicle independent formulation in which all masses are referenced to the initial spacecraft mass was employed. The power level and jet exhaust speed were optimized to yield maximum net spacecraft to initial mass ratio. Data were generated for a baseline specific propulsion system mass of 5 kg/kw with sensitivity data cases being run for specific masses up to 40 kg/kw. A propellant tankage factor of 0.03 was assumed throughout. Comparison data obtained from the QUICKTOP program were provided by the Technical Monitor.

2. Formulation.

The optimal trajectory and performance data for this study were obtained with the Heliocentric Interplanetary Low-Thrust Trajectory Optimization Program (HILTOP)[5]. This program utilizes the indirect variational calculus method for optimizing a three-dimensional low thrust heliocentric trajectory between assumed massless bodies moving in prescribed orbits about the sun. An analytic ephemeris is employed which yields orbital positions in a heliocentric ecliptic frame of date. The orbital elements of Earth are expressed as quadratic functions of Julian century in this frame. The assumed constant elements for the comet Encke in the 1980 apparition are as follows:

$a = 2.218$ AU	$e = 0.847$	$i = 11.95$ deg
$\omega = 185.98$ deg	$\Omega = 334.19$ deg	$\tau = 2444580$ (Dec. 6, 1980)

A trajectory is obtained by numerical integration of the equations of motion

$$\ddot{R} = h_\sigma \frac{a_o}{\nu} \frac{\Lambda}{\lambda} - \frac{\mu}{r^3} R$$

$$\dot{\nu} = - h_\sigma \frac{a_o}{c} ,$$

simultaneously with the adjoint equations

$$\ddot{\Lambda} = \frac{3\mu}{r^5} (R \cdot \Lambda) R - \frac{\mu}{r^3} \Lambda$$

$$\dot{\lambda}_\nu = h_\sigma \frac{a_o}{\nu^2} \lambda .$$

The step function h_σ is chosen on the basis of the sign of the switch function $\sigma = \lambda - \frac{\nu}{c} \lambda_\nu$ as follows:

$$h_\sigma = \begin{cases} 0 \text{ if } \sigma < 0 \\ 1 \text{ if } \sigma > 0 \end{cases} .$$

The initial position used to start the integration is that of Earth on the specified launch date, while the initial velocity is set equal to the velocity of Earth plus the specified hyperbolic excess speed applied in the direction of the primer vector, Λ. The initial mass ratio ν is, of course, equal to one, and the initial values of Λ, $\dot{\Lambda}$, and λ_ν are all guessed. The integration is terminated upon reaching the desired flight time.

An optimum trajectory for a specified trajectory class, flight time, and launch excess speed is obtained by solving the boundary value problem for a_o, c, and the initial values of Λ, $\dot{\Lambda}$, and λ_ν to yield the desired final position and velocity, and to satisfy the three transversality conditions

$$\lambda_\nu (t_f) = 1 + k_t$$

$$\lambda_{a_o} (t_f) = m_{ps}/a_o$$

$$\lambda_c(t_f) = -m_{ps}\left(\frac{1}{c} - \frac{\eta'}{\eta}\right)$$

where λ_{a_o} and λ_c are obtained by numerical integration of the equations

$$\dot{\lambda}_{a_o} = -h_\sigma \frac{\sigma}{\nu}$$

$$\dot{\lambda}_c = -h_\sigma \frac{a_o}{c^2}\lambda_\nu .$$

The initial values of both λ_{a_o} and λ_c are zero. Of course, the desired final position and velocity is taken to be that of comet Encke on the specified arrival date.

The powerplant is assumed to deliver a constant power p_o to the power conditioner. A single efficiency factor, η, is employed to relate beam power to the input power as follows:

$$p_b = \eta p_o ,$$

with η assumed to be a function of the jet exhaust speed.

$$\eta = \frac{b c^2}{c^2 + d^2} .$$

The values of the constant coefficients b and d used in this study were 0.842 and 16 km/sec, respectively. The thrusters are assumed to operate at constant jet exhaust speed and mass flow rate throughout all propulsive maneuvers. The dynamic relationships that apply during thruster operations are:

$$p_b = -\frac{1}{2}\dot{m} c^2 = \eta p_o$$

$$f = -\dot{m} c = a_o m_o .$$

Since the mass flow rate is assumed constant the spacecraft mass and mass ratio are linearly decreasing functions of propulsion time.

The spacecraft is assumed to consist of propulsion system, propellant and tankage. Any additional mass available is termed net spacecraft mass. Thus, in terms of mass ratios

$$\nu_{ps} + \nu_p + \nu_t + \nu_n = 1$$

where

$$\nu_{ps} = \alpha p_o / m_o = \alpha a_o c / 2\eta$$

$$\nu_t = k_t \nu_p .$$

Hence,

$$\nu_n = 1 - \alpha a_o c/2\eta - (1+k_t)\,\nu_p ,$$

which is to be maximized in the optimization procedure.

Other relationships that are necessary for comparison of results with those of the QUICKTOP program are the energy factor

$$J = \int_{t_o}^{t_f} a^2\, dt = a_o\, c\, \nu_p / (1-\nu_p) ,$$

and the geometric mean thrust acceleration

$$\bar{a} = (a_o a_f)^{\frac{1}{2}} = a_o / \sqrt{1-\nu_p} .$$

A useful relationship that results from the constant mass flow rate yields the propulsion time as a function of J and $\bar{a}$:

$$t_p = J/\bar{a}^2 .$$

3. Results.

Optimal trajectories for the Encke rendezvous mission in the flight time range of 400-1400 days may be divided into four distinct trajectory classes. These different classes arise because the same geometric configuration for transfers from Earth to the position Encke occupies on the desired arrival date repeats annually. Given a trajectory with a specified flight time, there will exist another trajectory with exactly the same travel angle and arrival date but with a flight time exactly one year longer. The longer flight time of one year is achieved by simply increasing the aphelion distance through which the trajectory passes. The sketch in Figure 1 depicts trajectories in each of the four classes that were considered in this study. The sketch depicts four trajectories arriving at Encke on the same arrival date and departing Earth at the same heliocentric location, but on dates exactly one year apart. The earlier launch dates (and hence the longer flight time) correspond to the larger aphelion distance. Hereafter, the terms short, intermediate, long and extra long flight time class will be used to differentiate among the four trajectory classes.

For each of the flight time classes, tables are presented which list the optimal values of six parameters as a function of launch excess speed and flight time. The six parameters include the energy parameter J, the propulsion time to flight time ratio t_p/t_f, the mean thrust acceleration $\bar{a}$, the power to mass ratio p_o/m_o, the net spacecraft mass ratio m_n/m_o $(=\nu_n)$, and the jet exhaust speed c. The values presented are those obtained from the HILTOP program. When available a corresponding data point obtained from the QUICKTOP program is included in parentheses.

In Table 1 are presented the data for the short flight time class. The table is divided into six parts which are labeled 1a through 1f and which contain the parameters J, t_p/t_f, $\bar{a}$, p_o/m_o, ν_n, and c, respectively. Each parameter is tabulated as a function of launch excess speeds at increments of 1 km/sec over

the range 0-8 km/sec and as a function of flight time at 50 day increments over the range 400-600 days. The only comparison points available for this class of solutions were at a flight time of 400 days. This comparison indicates relatively minor discrepancies between the two methods of solution, the largest being in the energy factor J which varies from 5-10 percent. It is particularly interesting to note that this discrepancy in J is not matched by a corresponding discrepancy in the net spacecraft mass ratio. This is easily explained as follows. Letting δJ denote a discrepancy in J and $\delta \nu_p$ a discrepancy in the propellant mass ratio ν_p, then one would expect that

$$\delta \nu_p = \frac{\partial \nu_p}{\partial J} \delta J$$

and since

$$\nu_p = \frac{J}{a_o c + J} ,$$

then, neglecting any discrepancies in a_o and c, and noting that $\delta \nu_n \cong - \delta \nu_p$ one obtains

$$\delta \nu_n = - \frac{a_o c}{(a_o c + J)^2} \delta J .$$

For the problem at hand, $a_o c$ and J are about equal and of magnitude 50 m^2/sec^3. Consequently, $\delta \nu_n$ should be about two orders of magnitude less than δJ, which is close to the difference exhibited in the tables.

In Table 2 are presented the data for the intermediate flight time class. The organization of the data is the same as for Table 1 with flight times at 50 day increments in the range 550-700 days and at 100 day increments thereafter to 900 days. The grid points for this class which yield direct comparisons of the HILTOP and QUICKTOP results indicate differences of 5-10 percent in J, $\bar{a}$, and c and of about 1-4 percent in net spacecraft mass ratio. A certain consistency is evident in the comparisons in that the QUICKTOP results are always

lower in J and $\bar{a}$ and higher in ν_n and c than the corresponding results of HILTOP. The most obvious discrepancy in the results of the two programs is in the propulsion time ratio. Whereas the QUICKTOP program indicates continuous propulsion to be optimum in all but one of the 14 grid points shown, the HILTOP program yields propulsion time ratios varying from about 0.6 to 0.9. Clearly, since the QUICKTOP yields more favorable performance estimates on the basis of optimal propulsion time, the difference in the output of the two programs would widen if HILTOP were constrained to continuous thrust solutions. For example, a few typical cases run with HILTOP indicated that forced continuous thrust resulted in a 2-5 percent increase in J and 0.5-1 percent decrease in ν_n as compared to optimal propulsion time results. The cases considered included flight times of 600, 700, and 800 days at a launch excess speed of zero. The optimal propulsion time ratios for these cases were about 0.85 (see Table 2b).

The long flight time class data are presented in Table 3 at 100 day increments in flight time over the range 900-1300 days. The results of the two programs compare more closely for this trajectory class than for the intermediate flight time class. With few exceptions, the results for this class are within two percent. Differences in propulsion time ratio, if they exist, are not so noticeable in this case because both programs yield continuous propulsion solutions at most of the grid points available for comparison. Similarly in Table 4, the single point available from QUICKTOP for the extra long flight time class compares very favorably with that from HILTOP. A difference of about two percent may be noted in J and c. The vacant grid points in Tables 1-4 are due to numerical problems experienced with HILTOP when attempting to attain those specific optimum trajectories.

To facilitate an understanding of the behavior and trends of the data presented in the tables, plots were prepared of the parameters J, $\bar{a}$ and t_p/t_f as functions of both the flight time and the launch excess speed. The three parameters are shown in Figures 2-4, respectively, as functions of flight time for

curves of selected launch excess speeds. These figures were prepared with the flight time plotted on a linear rather than the logarithmic scale suggested in the Statement of Work. The reasons for this choice were that launch opportunities repeat annually, which suggests a linear scale, and that compressing data at the longer flight times appeared to amplify rather than reduce problems one would have in curve fitting the data.

The results in Figures 2-4 are not particularly favorable from the standpoint of curve fitting for the QUICKLY program. One will note for both J and $\bar{a}$ that the general shapes of the curves change drastically from one trajectory class to the next and, to a lesser extent, from one excess speed to another. This would suggest potential difficulty in finding an acceptable general form of an equation to which the data may be accurately curve fitted. Figure 4 showing the propulsion time ratio has even more scatter. Here, with one exception, no attempt was made to fare curves through the data points. The linear dashed lines between data points are included to facilitate distinguishing the class of solutions to which each point belongs. Sufficient detail was developed to define the shape of the curve of propulsion time ratio versus flight time for an excess speed of 8 km/sec in the long flight time class and the results are shown by the solid curve in the Figure 4. The curve exhibits six distinct arcs within the flight time range 900-1200 days. From 900-920 days, the ratio changes very rapidly from about 0.73 to 1.0; from 920-940 the solution indicates continuous propulsion; from 940-980 the ratio is parabolic in shape, exhibiting a minimum value of about 0.85; and from 980-1200 there are three nearly linear segments with abrupt changes in slope at about 1080 and 1125 days. This rather unusual and unexpected shape was deduced from observations of the switch function time histories associated with the eight available data points along the curve. These time histories are shown in Figure 5.

To understand Figure 5, one must first realize that the switch function σ is used to optimally switch the engine on or off when it passes through zero. When

$\sigma < 0$, the engine is off and, conversely, when $\sigma > 0$, the engine is on. This figure is useful in understanding the propulsion time ratio curve in Figure 4 in that it shows the duration and location of individual coast phases in each solution. For example, the 900 day solution exhibits a negative switch function for about 240 days starting at Julian date 4130. At all other points, the switch function is positive. The minimum on the 910 day curve is shifted upward and to the right such that the coast phase is reduced to about 180 days. Otherwise, the curve closely resembles that for the 900 day case. Proceeding to the 920 day solution, one will note that the minimum has shifted further to the right and also upward to the extent that the function is always positive which yields the propulsion time ratio of one as seen in Figure 4. Meanwhile, with increasing flight time, a minimum of the switch function has developed early in the flights, around the Julian date 3700 for the 920 day case. For the 950 day case, it is seen that the late minimum has all but disappeared while the early minimum is noticeably more pronounced and has dropped below zero. Thus, the continuous thrust solutions are only optimal for a small flight time range of about 920-940 days. As the flight time increases above 940 days, the early minimum dips well below zero, resulting in a sizeable coast phase, and then quickly returns to near zero to give the parabolic dip shown in Figure 4. The minimum then hugs the zero line as is seen in the Figure 5 for flight times of 1000, 1050 and 1100 days. The minimum raises above the zero axis for the 1200 day solution, thereby eliminating that coast phase. This is the source of the abrupt change in slope of the curve in Figure 4 at a flight time of about 1125 days. The change in slope at about 1080 days is due to the new coast phase that is introduced in the solutions at launch and is first evident in the curves in Figure 5 for the 1100 day case. Thus, the unusual shape of the propulsion time curves as a function of flight time are seen to result from the rapid changes in the switch function time histories as the flight time is varied. If the curves of Figure 5 were drawn in perspective with flight time as the third coordinate, one would observe a rather complex surface resembling a rough terrain with high mountains and deep valleys. With this picture

in mind it then becomes somewhat easier to accept the erratic behavior of the propulsion time curves shown in Figure 4. The lesson to be learned from this example is that the propulsion time ratio must be considered (at least for the Encke rendezvous mission) as a rapidly fluctuating variable that does not lend itself well to a curve fitting approach.

The parameters J, $\bar{a}$ and t_p/t_f are plotted as functions of launch excess speed in Figures 6-8, respectively. These curves are seen to be quite smooth functions of the independent parameter and should be somewhat more amenable to curve fitting than the corresponding curves plotted as a function of flight time. The parameters J and $\bar{a}$ for long flight times within each class appear to match quite favorably a linear curve fit on the semi-log grid over the range of launch v_∞'s shown. The shorter flight times in each class (e.g., 900 days-long and 1300 days-extra long) will probably require a higher order fit. It is particularly interesting to note the striking similarity in the shapes of the curves for J and $\bar{a}$. It would appear that identical functional forms could be used for the two variables. Because of this it is probably preferable to avoid curve fitting the propulsion time ratio since it may be immediately obtained from J and $\bar{a}$.

The sensitivities of J, $\bar{a}$ and t_p/t_f to the specific propulsion system mass α were obtained for several selected cases in the intermediate flight time class. For a 700 day mission solutions were obtained for several values of α in the range 5-40 kg/kw and for launch excess speeds from 0-8 km/sec. In addition, cases were obtained for the same interval in α holding the launch excess speed fixed at 4 km/sec and varying the flight time in the range 600-800 days. The resulting variations in the parameters J, $\bar{a}$ and t_p/t_f are presented graphically in Figures 9-11, respectively. Although somewhat non-linear, these curves are very smooth functions of α, implying little difficulty in curve fitting the data if desired. The smoothness in the data also indicates that choosing a different nominal value of α for the generation of the basic data in QUICKLY would not influence the degree of difficulty in curve fitting data as a function of flight time.

4. Concluding Remarks.

From the data generated for the Encke rendezvous mission in this study, it is possible to draw the following conclusions regarding the curve fitting of the data in QUICKLY:

1. Curve-fits as a function of flight time must be restricted to relatively short arcs within each class of solutions if accurate propulsion time estimates are required. Concomitant with this requirement will be the need for initially generating the optimal trajectory data on a small flight time grid ($\sim$ 10 days). Performance estimates without regard to propulsion time may be obtained on a somewhat larger grid ($\sim$ 50 days). Depending upon the accuracy desired, it may be necessary to choose different functional forms for the curve fit for the different classes of solutions and possibly for the different excess speeds within a class.

2. Of the three parameters J, $\bar{a}$ and t_p/t_f, only two are independent, and since J and $\bar{a}$ appear to be smoother functions of both flight time and launch excess speed, it is recommended that they be chosen for curve fitting.

3. Curve fits of J and $\bar{a}$ as functions of launch excess speed or specific propulsion system mass for a given flight time may be adequately achieved with low order equations that apply over the entire ranges of v_∞ and α investigated in this study. In many cases a linear fit on a semi-log grid is appropriate.

A comparison of the data generated in this study with that generated with the QUICKTOP program and supplied by the Technical Monitor leads to the following conclusions for the specific mission investigated:

1. The net spacecraft mass ratios obtained from the QUICKTOP and HILTOP programs for the same case compare very favorably, usually differing by less than one percent.

2. Parameters such as J, $\bar{a}$ and c usually compare within 10 percent and frequently within 5 percent.

3. Propulsion time ratio appeared to be the parameter in which the greatest discrepancies existed in the results of the two programs. The largest discrepancies occurred for the intermediate flight time class for which QUICKTOP generally predicted continuous thrust whereas HILTOP predicted propulsion times of 60-90 percent of the flight time.

CONSIDERATIONS OF QUICKLY

A second, and essentially independent, task of this study was to review the design of the program QUICKLY and to suggest changes to the program which would extend its capability and/or improve its accuracy while retaining its desirable attributes of simplicity and speed of operation. Briefly, the manner in which QUICKLY currently operates, as described in Reference 4, is as follows. Stored in data arrays are coefficients of specific polynomials which yield the performance parameters J and t_p as a function of the flight time and the sum of the launch and arrival excess speeds (launch excess speed only for flyby missions) for specific missions of interest. These coefficients were determined independently from least squares curve fits of precomputed optimal trajectory data generated with open power and jet exhaust speed to yield maximum net spacecraft mass ratio for specified values of α, k_t and any other structural factors. Given J and t_p for specified flight time and set of hyperbolic excess speeds, analytic equations are then entered which allow one to compute the optimum values of the spacecraft parameters such as c, a_o, ν_{ps}, $\bar{a}$, etc., in closed form. Thus, it is not necessary to curve fit these spacecraft parameters as they are not independent. Empirical relations are then employed to obtain estimates of the changes in performance and spacecraft parameters due to changes in design parameters, such as α, and due to the imposition of constraints, such as fixed power and/or limited propulsion time. The empirical equations used to handle the constraints involve variations of Zola's characteristic length[6] method which assumes invariance of the characteristic length for a specific mission over a wide range of system parameters. The characteristic length is, roughly, the second integral of the thrust acceleration.

Except for the extent to which precomputed mission data is stored and available in the program, the greatest limitations in QUICKLY would appear to come from two sources: (1) the accuracy to which the precomputed data are

curve fitted, and (2) the validity of the empirical relations employed. Each of these sources will now be considered with specific attention being given to the numerical results obtained for the Encke mission described in the preceding section. One additional factor which has nothing to do with the design of QUICKLY but which would appear to represent a limitation in QUICKLY is the accuracy of the precomputed data itself.

The range of flight times and number of classes of solutions considered in this study for the Encke rendezvous mission undoubtedly exceed those for which QUICKLY was originally envisioned to handle. This supposition combined with the fact that the Encke mission requires relatively large changes in inclination and eccentricity should be sufficient reason to suspect that the optimal performance data for the Encke mission may not be as well behaved as, say, a mission to one of the planets, and hence may present more severe problems in curve fitting the data. This is indeed the case as is obvious in Figures 2-4. Little can be stated conclusively in this report concerning explicit curve fitting techniques to adequately handle the Encke rendezvous mission because the scope of work did not permit sufficient in-depth study to cover this aspect of the problem. However, due to the striking similarity of the curves of J and $\bar{a}$, as is seen in Figures 2, 3, 6 and 7, and due to the erratic behavior of the propulsion time ratio curves, a study of techniques for curve fitting J and $\bar{a}$ rather than J and t_p seems warranted. Such a study should include an examination of the resultant error in t_p and the implications of the error as it affects the characteristic length relations and appropriate procedures to follow when the calculated t_p is greater than t_f.

The use of empirical equations to describe relations among a set of variables carries with it a certain amount of risk in that one can only be certain that it applies over the ranges of the variables that were used in deriving the equations. This is particularly true if the functional form of the relationship was derived from a numerical rather than an analytic basis. If the assumed form of the equation incorrectly describes the relationship, erroneous results will obviously be obtained from the use

of the empirical equation. A pertinent example of this is found in the data presented in the preceding section. In Figure 9, the behavior of J as a function of α is shown for five different flight time/launch excess speed combinations. In four of the five cases the slopes of the curves at $\alpha = 5$ are negative. The empirical equation appearing in QUICKLY which is intended to describe the variation in J as α is varied will not account for a change of sign of slope.

The use of the characteristic length equations also represents an empirical approach. Furthermore, a number of additional empirical relations were developed for QUICKLY, again based on numerical observations, which attempt to correct the characteristic length to account for various mission constraints. Because of a lack of knowledge as to the scope of the cases observed in deriving these corrections, there is some question regarding the general applicability of the equations. A method is available that appears to eliminate the need for empirical scaling to cover constrained power cases or variations in α. The method also has other attributes as well as some disadvantages. The remainder of this report is devoted to a discussion of this method.

Recently a concept was published[7] which describes an approach and a set of assumptions under which one may generate optimal trajectory data that is independent of the launch vehicle, the power level, the specific powerplant mass and the propulsion system efficiency. Here the term independent implies that the optimum trajectory may be defined without regard to any of the four parameters and therefore effects of variations of any or all of the parameters on the performance may be determined exactly without regard to any approximate or empirical formulas. These features are achievable by redefining what is meant by an optimal trajectory. The optimal data discussed in the preceding section was generated under the criterion of maximizing the net mass ratio with open power and jet exhaust speed and specified launch and arrival dates and hyperbolic excess

speeds. The independence cited above is achieved by declaring the performance index to be the net mass to power ratio m_n/p_o rather than the net mass ratio. Although this may seem on the surface to be a somewhat contrived requirement, it actually proves to be the best choice of the performance index for some cases of interest - specifically those for which the power level is constrained to a level well below that which yields the true maximum net mass for a given launch vehicle. This is seen to be true from the following discussion.

Suppose a mission to a given target is specified in terms of the launch and arrival dates and hyperbolic excess speeds, and several trajectories for a range of values of the power p_o are optimized to yield maximum net spacecraft mass. We will assume that the same initial mass, corresponding to the payload capability of a selected launch vehicle at the specified launch excess speed, is used at all power levels, and also assume that the jet exhaust speed is optimized at each power level. Then a typical plot of the maximum net spacecraft mass as a function of power level will appear as shown by the solid curve in the sketch of Figure 12. The absolute maximum of m_n occurs at a power level of $p_{o_{opt}}$ whereas the maximum value of the ratio m_n/p_o occurs at a power level p_o^* corresponding to the tangency point of the dashed line extending from the origin and the solid curve. An interesting property of optimal solutions with constrained power was noted independently by Meissinger[8] and Zola[9]. This property may be observed in Figure 12 by noting that at power levels below p_o^*, a larger net spacecraft mass can be achieved by following the linear dashed line than by following the solid curve. To follow the dashed line requires that one employ the jet exhaust speed of the tangency point and scale proportionately the power level and all mass components. If this is done, the trajectory followed will be the same for any point on the dashed curve. The reduced initial mass at any point on the dashed curve represents the optimum initial mass for the corresponding power level. Consequently, if a larger initial mass is used, the additional propellant and tankage requirements necessary to

meet the specified end conditions will exceed the increase in initial mass thereby causing a net reduction in the net spacecraft mass. Now, note that the tangency point of the dashed and solid curves represents the maximum of the ratio m_n/p_o that is achieved anywhere on the solid curve. It then follows that the choice of this ratio as the performance index will indeed yield the solution for maximum net spacecraft mass achievable for powers less than p_o^*.

To better understand how the approach is implemented in a mission study, suppose a set of optimal trajectories were obtained for maximum m_n/p_o over a range of launch excess speeds. For each value of launch excess speed there would result from the optimization corresponding optimal values of a_o and c as well as the propellant fraction ν_p and the propulsion time t_p. Of course, the parameters J and $\bar{a}$ are also available. Note that each of these parameters is invariant along the dashed curve of Figure 12. From the mass relations given in the preceding section for the Encke rendezvous mission one may write

$$\frac{m_n}{p_o} = \frac{2\eta}{a_o c}\left[1 - (1+k_t)\,\nu_p\right] - \alpha$$

$$\frac{m_o}{p_o} = \frac{2\eta}{a_o c} \; .$$

Now, due to the dependence of a_o, c and ν_p on launch v_∞, both m_n/p_o and m_o/p_o are also functions of v_∞. Suppose one now selects values of α, η and p_o and plots m_n as a function of launch v_∞ and selects the case (i.e., the v_∞) at which m_n is maximized. But from the equation for m_n/p_o it is clear that although the choice of α affects the value of m_n, it does not affect the value of v_∞ at which m_n is maximized. Similarly, a change in the value of p_o or η will affect only the magnitude of m_n and not the location of the maximum. Consequently one accounts exactly for any changes in these parameters through the above equations. Furthermore, to consider a specific launch vehicle, one simply

multiplies the function m_o/p_o $(=2\eta/a_o c)$ by the prescribed power. This, in effect, yields a curve of optimum initial mass as a function of launch v_∞. The intersection of this curve with that of the payload capability of the desired launch vehicle, plotted on the same scale, yields the appropriate launch excess speed and, in turn, the maximum net mass capability for the specified launch vehicle and power level. A maximum power level that one should attempt to use with this approach for a given launch vehicle may be determined by dividing the payload capability of the launch vehicle at a given launch v_∞ to obtain a curve of the optimum power level p_o^* for that launch vehicle as a function of launch v_∞. The peak of this curve represents a limit to the power level beyond which the optimum initial mass always exceeds the payload capability of the launch vehicle and hence no solution exists.

To further clarify the use of this multi-parameter independent mode (MPIM) a set of optimal data for a specific mission were generated. The mission chosen was the 700 day Encke rendezvous in the intermediate flight time class for which data are also available in the Table 2 for maximum net mass ratio. The performance data generated using the new mode are tabulated as a function of launch excess speed and are presented in Table 5. The parameters include all those presented in Table 2 for the same mission so that a direct comparison of the results of the two modes can be made. Such a comparison leads to the following observations:

(1) The energy factor J differs only slightly in the two approaches.

(2) The propulsion is continuous for the MPIM. This will not always be the case. However, longer propulsion times are expected to result in general using the MPIM.

(3) The power to mass ratio p_o/m_o is considerably smaller (by about a factor of 5) for the MPIM. Of course, in Table 5 p_o/m_o represents p_o^*/m_o whereas in Table 2 it represents $p_{o_{opt}}/m_o$.

(4) Similarly, because of the different power levels at which the points apply, the net mass ratio ν_n is much smaller for the MPIM,

(5) Possibly the most striking difference in the results of the two methods is in the jet exhaust speed c. Whereas the optimum value using the original method was over 120 km/sec, it is reduced to about 26 km/sec using the MPIM. This is because the reduction in power from $p_{o_{opt}}$ to p_o^* is achieved primarily by reducing the jet exhaust speed and only secondarily by reducing the thrust acceleration.

Data for the 700 day mission in Table 2 were employed to develop the NEP performance data for the Titan III D/Centaur launch vehicle. The data are presented in Figure 13 and include the initial NEP spacecraft mass (assumed equal to the payload capability of the launch vehicle), the optimum power $p_{o_{opt}}$ (equal to the ratio p_o/m_o from Table 2 multiplied by the initial mass), and the net spacecraft mass (equal to the product of ν_n and m_o). The parameters are plotted as a function of launch excess speed. The peak of the net mass curve corresponds to the solution generally obtained for this launch vehicle under the assumption of optimum power and jet exhaust speed. Note that if constrained power data is desired, it is essential to use the characteristic length technique to scale this data. Similarly empirical equations are required to approximate variations in these parameters due to changes in α or η. The data from Table 5 were used in developing corresponding curves in Figure 14 for the same launch vehicle implementing the MPIM. Plotted as a function of launch excess speed are the launch vehicle payload capability, the power level p_o^* for this launch vehicle, and the net mass associated with the power level p_o^*. In addition, dashed curves are presented for the case of power fixed at 15 kilowatts. Shown are the optimum initial mass for this power level and the net spacecraft mass associated with that solution. Note that these dashed lines intersect the corresponding solid lines and terminate at the launch excess speed for which $p_o^* = 15$ kilowatts. For all lesser excess

speeds the optimum initial mass is less than the payload capability of the launch vehicle, and for those cases the launch vehicle could be off-loaded. To consider a different α in this example, all that is required is to evaluate the difference in propulsion system weight and transfer to or from the net mass on a one-to-one basis. Similarly, a change in efficiency is accommodated by scaling the initial mass and the sum of the propulsion system and net masses by the ratio of the new to the old efficiency factor. Then subtracting the propulsion system mass from the scaled sum yields the new spacecraft mass.

The curve fitting of parameters for the MPIM should prove no more difficult than the original approach. No change in the choice of variables curve fitted is apparent at this time although that possibility should be considered. It will be necessary to re-derive the appropriate expression for optimal c, given J and t_p or $\bar{a}$, since the performance index has changed. An alternative is to generate optimum trajectory data for specified rather than optimal values of c and either curve fit the data as a function of c or use the characteristic length relations to approximate effects of changes in c. Similar alternatives exist with respect to constrained propulsion time. Finally, it is important to note that the MPIM is adaptable to other types of missions, such as orbiters and flybys, with no more difficulty than with the original approach. The principal limitation of the MPIM is that power levels should not exceed p_o*.

REFERENCES

[1] D. W. Hahn, F. T. Johnson and B. F. Itzen, "Chebychev Trajectory Optimization Program (CHEBYTOP)," Boeing Company Report No. D2-121308-1, July 1969.

[2] D. W. Hahn and F. T. Johnson, "Chebychev Trajectory Optimization Program (CHEBYTOP II)," Boeing Company Report No. D180-12916-1, June 1971.

[3] A. C. Mascy, "QUICKTOP, A User Oriented Multi-Option Computer Program for Quick Trajectory and Mass Optimization of Electric Propulsion Missions," OART/Advanced Concepts and Missions Division Working Paper MS-71-1, June 1971.

[4] A. C. Mascy, "A Computer Program for Quickly Analyzing Electric Propulsion Missions," NASA TM X-2004, April 1970.

[5] J. L. Horsewood, P. F. Flanagan and F. I. Mann, "HILTOP: Heliocentric Interplanetary Low Thrust Trajectory Optimization Program," Analytical Mechanics Associates, Inc. Report No. 71-38, November 1971.

[6] C. L. Zola, "A Method of Approximating Propellant Requirements of Low-Thrust Trajectories," NASA TN D-3400, 1966.

[7] T. A. Barber, J. L. Horsewood, and H. Meissinger, "Basic Parameters for Low Thrust Mission and System Analysis", AIAA Paper No. 72-426, presented at the 9th Electric Propulsion Conference, Bethesda, Md., April 17-19, 1972.

[8] "Common Solar-Electric Upper Stage for High Energy Unmanned Missions," Second Quarterly Progress Report and Briefing, TRW Systems Group, Redondo Beach, California, Document 16552-6003-TO-00, January 1971.

[9] C. L. Zola, "An Improved Method for Maximizing the Payload of Electric Propulsion Spacecraft at Low Power Level," NASA TM X-52980, February 1971.

Table 1a - Energy Factor, J (m^2/sec^3)
Short Flight Time Class

Launch v_∞ (km/sec)	Flight Time (days)				
	400	450	500	550	600
0	54.55 (50.3)	46.05	45.58	44.96	41.97
1	50.76	44.51	44.84	43.71	40.12
2	47.40	43.36	44.37	42.71	38.60
3	44.42	42.44	44.11	41.97	37.31
4	41.82 (41.4)	41.63		41.42	36.19
5	39.56	40.97		41.00	35.20
6	37.61 (41.4)	40.45		40.70	34.33
7	35.94	40.08		40.51	33.56
8	34.54 (31.0)	39.85		40.41	32.90

Table 1b - Propulsion Time Ratio, t_p/t_f
Short Flight Time Class

Launch v_∞ (km/sec)	Flight Time (days)				
	400	450	500	550	600
0	.7596 (.73)	.7633	.7180	.6915	.6946
1	.7610	.7597	.7078	.6829	.6908
2	.7599	.7572	.6997	.6771	.6870
3	.7565	.7373	.6942	.6887	.6830
4	.7515 (.72)	.7182		.6991	.6788
5	.7458	.7003		.7089	.6745
6	.7400 (.72)	.6840		.7184	.6700
7	.7347	.6695		.7273	.6722
8	.7304 (.72)	.6566		.7357	.6757

Table 1c - Mean Thrust Acceleration, $\bar{a}$, (10^{-4} m/sec^2)
Short Flight Time Class

Launch v_∞ (km/sec)	Flight Time (days)				
	400	450	500	550	600
0	14.41	12.46	12.12	11.70	10.80
1	13.89	12.28	12.11	11.61	10.58
2	13.43	12.14	12.12	11.52	10.41
3	13.04	12.17	12.13	11.32	10.27
4	12.69	12.21		11.17	10.14
5	12.39	12.27		11.03	10.03
6	12.13	12.33		10.92	9.94
7	11.90	12.41		10.83	9.81
8	11.70	12.49		10.75	9.69

Table 1d - Power to Mass Ratio, p_o/m_o (kw/kg)
Short Flight Time Class

Launch v_∞ (km/sec)	Flight Time (days)				
	400	450	500	550	600
0	.0518	.0490	.0483	.0481	.0474
1	.0508	.0484	.0483	.0480	.0469
2	.0498	.0479	.0483	.0478	.0464
3	.0489	.0477	.0483	.0476	.0461
4	.0480	.0476		.0475	.0457
5	.0472	.0475		.0473	.0454
6	.0466	.0474		.0473	.0451
7	.0460	.0474		.0472	.0448
8	.0454	.0474		.0472	.0446

Table 1e - Net Spacecraft Mass Ratio, m_n/m_o
Short Flight Time Class

Launch v_∞ (km/sec)	Flight Time (days)				
	400	450	500	550	600
0	.3337 (.335)	.3768	.3795	.3834	.4006
1	.3517	.3849	.3834	.3901	.4112
2	.3685	.3911	.3858	.3956	.4202
3	.3842	.3960	.3872	.3999	.4280
4	.3986 (.399)	.4003		.4032	.4350
5	.4117	.4039		.4056	.4412
6	.4234 (.425)	.4067		.4075	.4469
7	.4338	.4087		.4087	.4520
8	.4428 (.443)	.4099		.4094	.4565

Table 1f - Optimum Jet Exhaust Speed, c (km/sec)
Short Flight Time Class

Launch v_∞ (km/sec)	Flight Time (days)				
	400	450	500	550	600
0	74.45 (73)	80.08	81.25	83.94	88.92
1	74.95	79.90	81.09	83.89	89.19
2	75.32	79.73	80.88	83.95	89.41
3	75.55	78.95	80.72	84.92	89.57
4	75.70 (74)	78.18		85.74	89.67
5	75.78	77.43		86.48	89.72
6	75.84 (75)	76.72		87.17	89.73
7	75.90	76.05		87.81	90.10
8	75.99 (76)	75.42		88.39	90.52

Table 2a - Energy Factor, J (m^2/sec^3)
Intermediate Flight Time Class

Launch v_∞ (km/sec)	Flight Time (days)					
	550	600	650	700	800	900
0	23.28 (20.3)	12.75 (11.41)	10.81 (10.5)	10.41 (9.89)	9.82 (9.26)	9.71 (9.17)
1	17.76	10.52	10.20		9.47	9.24
2	13.34	9.59 (9.04)	9.62	9.32 (8.89)	9.13	8.87
3	9.96	8.94	9.05	8.85	8.84	8.67
4	8.39	8.37 (7.84)	8.51	8.41 (8.07)	8.60	8.61
5	7.63	7.88	8.00	7.98	8.39	
6	7.13	7.43 (7.00)	7.50	7.56 (7.29)	8.20	
7	6.70	7.03	7.03	7.16	8.00	
8	6.53	6.64 (6.25)	6.59	6.76 (6.35)	7.81	

Table 2b - Propulsion Time Ratio, t_p/t_f
Intermediate Flight Time Class

Launch v_∞ (km/sec)	Flight Time (days)					
	550	600	650	700	800	900
0	.6159 (1.0)	.8650 (1.0)	.8721 (1.0)	.8748 (1.0)	.8379 (1.0)	.8165 (1.0)
1	.6913	.8879	.8617		.7897	.7949
2	.8003	.8520 (1.0)	.8513	.8609 (1.0)	.7440	.7681
3	.9889	.8357	.8409	.8512	.7216	.7492
4	.9014	.8230 (1.0)	.8305	.8424 (1.0)	.7105	.7293
5	.8228	.8108	.8200	.8338	.7013	
6	.7696	.7977 (1.0)	.8092	.8251 (1.0)	.6926	
7	.7209	.7824	.7983	.8164	.6842	
8	.7757	.7428 (.843)	.7871	.8075 (1.0)	.6756	

Table 2c - Mean Thrust Acceleration, $\bar{a}$ (10^{-4} m/sec^2)
Intermediate Flight Time Class

Launch v_∞ (km/sec)	Flight Time (days)					
	550	600	650	700	800	900
0	8.918	5.331 (4.70)	4.698	4.436 (4.05)	4.118 (3.66)	3.911 (3.44)
1	7.352	4.781	4.592		4.165	3.867
2	5.922	4.661 (4.07)	4.485	4.231 (3.83)	4.214	3.853
3	4.604	4.542	4.379	4.145	4.209	3.857
4	4.424	4.430 (3.89)	4.272	4.062 (3.65)	4.186	3.897
5	4.418	4.330	4.167	3.978	4.161	
6	4.414	4.240 (3.68)	4.063	3.893 (3.48)	4.138	
7	4.422	4.162	3.961	3.807	4.114	
8	4.209	4.153 (3.78)	3.861	3.720 (3.29)	4.089	

Table 2d - Power to Mass Ratio, p_o/m_o (kw/kg)
Intermediate Flight Time Class

Launch v_∞ (km/sec)	Flight Time (days)					
	550	600	650	700	800	900
0	.0437	.0337	.0304	.0299	.0293	.0290
1	.0391	.0302	.0297		.0290	.0284
2	.0345	.0289	.0290	.0287	.0287	.0279
3	.0300	.0280	.0283	.0282	.0284	.0276
4	.0273	.0273	.0276	.0276	.0281	.0275
5	.0263	.0266	.0269	.0270	.0278	
6	.0256	.0259	.0262	.0264	.0276	
7	.0251	.0254	.0255	.0258	.0273	
8	.0248	.0248	.0248	.0252	.0270	

Table 2e - Net Spacecraft Mass Ratio, m_n/m_o
Intermediate Flight Time Class

Launch v_∞ (km/sec)	Flight Time (days)					
	550	600	650	700	800	900
0	.5284 (.558)	.6397 (.657)	.6657 (.673)	.6715 (.679)	.6803 (.688)	.6821 (.690)
1	.5812	.6696	.6743		.6854	.6892
2	.6317	.6830 (.691)	.6829	.6876 (.694)	.6905	.6949
3	.6777	.6931	.6915	.6950	.6950	.6981
4	.7018	.7020 (.710)	.7000	.7020 (.707)	.6987	.6989
5	.7142	.7101	.7085	.7090	.7021	
6	.7229	.7178 (.725)	.7168	.7160 (.720)	.7052	
7	.7305	.7250	.7251	.7232	.7084	
8	.7339	.7319 (.739)	.7332	.7304 (.734)	.7117	

Table 2f - Optimum Jet Exhaust Speed, c (km/sec)
Intermediate Flight Time Class

Launch v_∞ (km/sec)	Flight Time (days)					
	550	600	650	700	800	900
0	92.3 (114)	115.7 (121)	117.8 (125)	122.9 (131.9)	129.5 (143.5)	134.9 (151.5)
1	98.5	115.0	117.4		126.2	133.3
2	106.6	112.1 (122.8)	117.0	123.0 (131.5)	123.0	131.2
3	118.2	111.1	116.6	122.7	121.6	129.5
4	111.0	110.5 (117.5)	116.1	122.4 (128.6)	120.9	127.8
5	106.3	109.9	115.7	122.1	120.3	
6	103.2	109.3 (128.3)	115.2	121.7 (132.1)	119.7	
7	100.4	108.5	114.7	121.3	119.1	
8	104.3	106.1 (112.9)	114.2	121.0 (134.1)	118.5	

Table 3a - Energy Factor, J (m^2/sec^3)
Long Flight Time Class

Launch v_∞ (km/sec)	Flight Time (days)				
	900	1000	1100	1200	1300
0	36.75		(4.83)	4.89 (4.68)	4.29
1	29.09			4.55	3.70
2	22.56	(4.013)	4.40	4.25	
3	17.06		4.22	4.03	
4	12.53	2.34 (2.195)	4.07	3.84	
5	8.88	1.86	3.92	3.67	
6	6.04 (5.78)	1.56 (1.515)	3.77	3.51	
7	3.94	1.33	3.63	3.36	
8	2.49 (2.455)	1.13 (1.094)	3.48	3.20	

Table 3b - Propulsion Time Ratio, t_p/t_f
Long Flight Time Class

Launch v_∞ (km/sec)	Flight Time (days)				
	900	1000	1100	1200	1300
0	.5146		(1.0)	.9883 (.931)	.9165
1	.5267			.9488	.8610
2	.5433	(1.0)	1.0	.9129	
3	.5640		.9928	.8885	
4	.5889	1.0 (1.0)	.9837	.8772	
5	.6180	1.0	.9718	.8698	
6	.6518 (.703)	1.0 (1.0)	.9610	.8634	
7	.6908	1.0	.9510	.8574	
8	.7350 (.702)	.9804 (1.0)	.9416	.8514	

Table 3c - Mean Thrust Acceleration, $\bar{a}$ (10^{-4} m/sec^2)
Long Flight Time Class

Launch v_∞ (km/sec)	Flight Time (days)				
	900	1000	1100	1200	1300
0	9.58		(2.26)	2.19 (2.20)	2.04
1	8.43			2.15	1.96
2	7.31	(2.15)	2.15	2.12	
3	6.24		2.11	2.09	
4	5.23	1.64 (1.59)	2.09	2.06	
5	4.30	1.47	2.06	2.02	
6	3.45 (3.25)	1.34 (1.32)	2.03	1.98	
7	2.71	1.24	2.00	1.94	
8	2.09 (2.12)	1.16 (1.125)	1.97	1.91	

Table 3d - Power to Mass Ratio, p_o/m_o (kw/kg)
Long Flight Time Class

Launch v_∞ (km/sec)	Flight Time (days)				
	900	1000	1100	1200	1300
0	.0512			.0220	.0208
1	.0471			.0213	.0194
2	.0428		.0210	.0207	
3	.0384		.0206	.0202	
4	.0338	.0159	.0203	.0198	
5	.0292	.0142	.0200	.0194	
6	.0247	.0130	.0196	.0190	
7	.0203	.0121	.0193	.0186	
8	.0164	.0112	.0189	.0182	

Table 3e - Net Spacecraft Mass Ratio, m_n/m_o
Long Flight Time Class

Launch v_∞ (km/sec)	Flight Time (days)				
	900	1000	1100	1200	1300
0	.4313		(.770)	.7690 (.773)	.7828
1	.4837			.7768	.7973
2	.5366	(.789)	.7802	.7836	
3	.5896		.7844	.7891	
4	.6423	.8372 (.841)	.7882	.7937	
5	.6941	.8540	.7918	.7981	
6	.7440 (.749)	.8658 (.867)	.7955	.8023	
7	.7906	.8760	.7993	.8065	
8	.8318 (.831)	.8851 (.887)	.8032	.8107	

Table 3f - Optimum Jet Exhaust Speed, c (km/sec)
Long Flight Time Class

Launch v_∞ (km/sec)	Flight Time (days)				
	900	1000	1100	1200	1300
0	105.4		(169.5)	179.0 (174.3)	180.1
1	108.0			175.9	174.6
2	111.1	(163.6)	173.1	172.7	
3	114.5		172.6	170.5	
4	118.3	167.9 (157.5)	171.9	169.5	
5	122.4	167.4	171.0	168.9	
6	126.8 (131.0)	167.6 (164.9)	170.2	168.4	
7	131.6	167.8	169.5	167.9	
8	136.8 (118.4)	166.5 (167.5)	168.9	167.5	

Table 4a - Energy Factor, J (m^2/sec^3)
Extra Long Flight Time Class

Launch v_∞ (km/sec)	Flight Time (days)		
	1300	1350	1400
0	25.13		
1	19.44		
2	14.58		
3	10.51		
4	7.20		
5	4.59		1.62
6	2.63		1.30 (1.276)
7	1.29	.41	1.10
8	.51	.29	.93

Table 4b - Propulsion Time Ratio, t_p/t_f
Extra Long Flight Time Class

Launch v_∞ (km/sec)	Flight Time (days)		
	1300	1350	1400
0	.4219		
1	.4204		
2	.4267		
3	.4400		
4	.4609		
5	.4912		1.0
6	.5344		1.0 (1.0)
7	.5947	1.0	1.0
8	.6655	.9981	1.0

Table 4c - Mean Thrust Acceleration, $\bar{a}$ (10^{-4} m/sec^2)
Extra Long Flight Time Class

Launch v_∞ (km/sec)	Flight Time (days)		
	1300	1350	1400
0	7.28		
1	6.42		
2	5.51		
3	4.61		
4	3.73		
5	2.88		1.16
6	2.09		1.04 (1.027)
7	1.39	.59	.95
8	.82	.50	.88

Table 4d - Power to Mass Ratio, p_o/m_o (kw/kg)
Extra Long Flight Time Class

Launch v_∞ (km/sec)	Flight Time (days)		
	1300	1350	1400
0	.0448		
1	.0406		
2	.0362		
3	.0316		
4	.0268		
5	.0219		.0134
6	.0170		.0120
7	.0121	.0069	.0111
8	.0077	.0058	.0102

Table 4e - Net Spacecraft Mass Ratio, m_n/m_o
Extra Long Flight Time Class

Launch v_∞ (km/sec)	Flight Time (days)		
	1300	1350	1400
0	.5151		
1	.5658		
2	.6175		
3	.6698		
4	.7224		
5	.7751		.8636
6	.8273		.8774 (.878)
7	.8777	.9304	.8871
8	.9225	.9413	.8957

Table 4f - Optimum Jet Exhaust Speed, c (km/sec)
Extra Long Flight Time Class

Launch v_∞ (km/sec)	Flight Time (days)		
	1300	1350	1400
0	117.7		
1	118.9		
2	121.1		
3	124.3		
4	128.5		
5	133.9		200.4
6	140.8		200.1 (195)
7	149.7	198.5	200.3
8	159.3	198.5	200.6

Table 5 - Performance Parameters for 700 Day Encke Rendezvous Mission
Multi-parameter Independent Mode
Arrival on October 17, 1980

Launch v_∞ km/sec	J m^2/sec^3	t_p/t_f	$\bar{a}$ 10^{-4} m/sec^2	p_o/m_o kw/kg	ν_n	c km/sec	m_n/p_o kg/kw
0	10.355	1.0	4.1379	.0059075	.37285	27.946	63.115
1	9.890	1.0	4.0438	.0057949	.37938	27.776	65.467
2	9.441	1.0	3.9510	.0056625	.38462	27.493	67.924
3	9.000	1.0	3.8576	.0055248	.38970	27.179	70.536
4	8.564	1.0	3.7630	.0053844	.39485	26.849	73.332
5	8.134	1.0	3.6673	.0052425	.40014	26.508	76.327
6	7.710	1.0	3.5704	.0050992	.40562	26.159	79.545
7	7.292	1.0	3.4723	.0049551	.41130	25.802	83.006
8	6.881	1.0	3.3731	.0048101	.41721	25.438	86.736

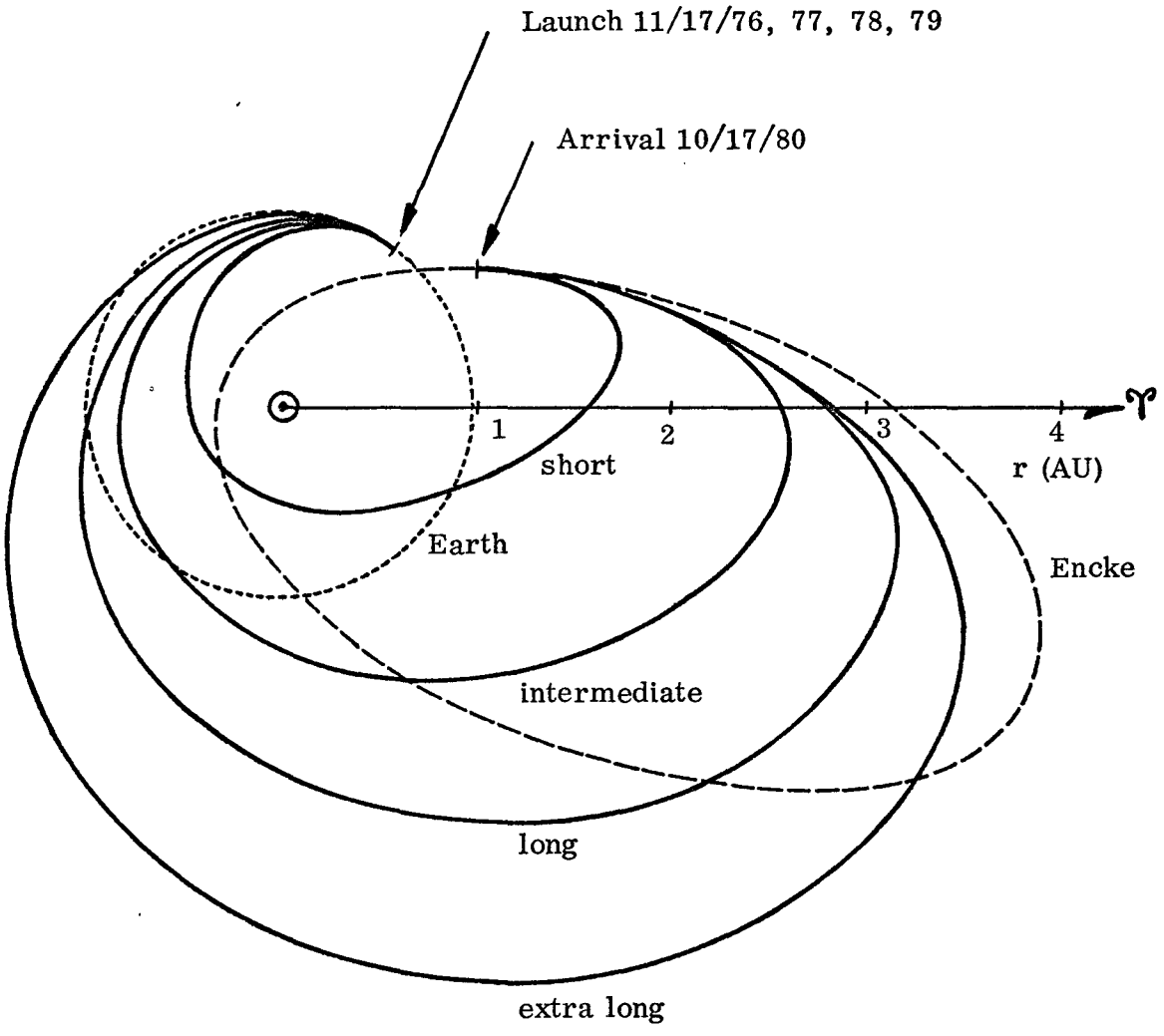

Figure 1 - Typical trajectory profiles for four trajectory classes.

1980 NEP ENCKE RENDEZVOUS MISSION

Arrival on October 17, 1980

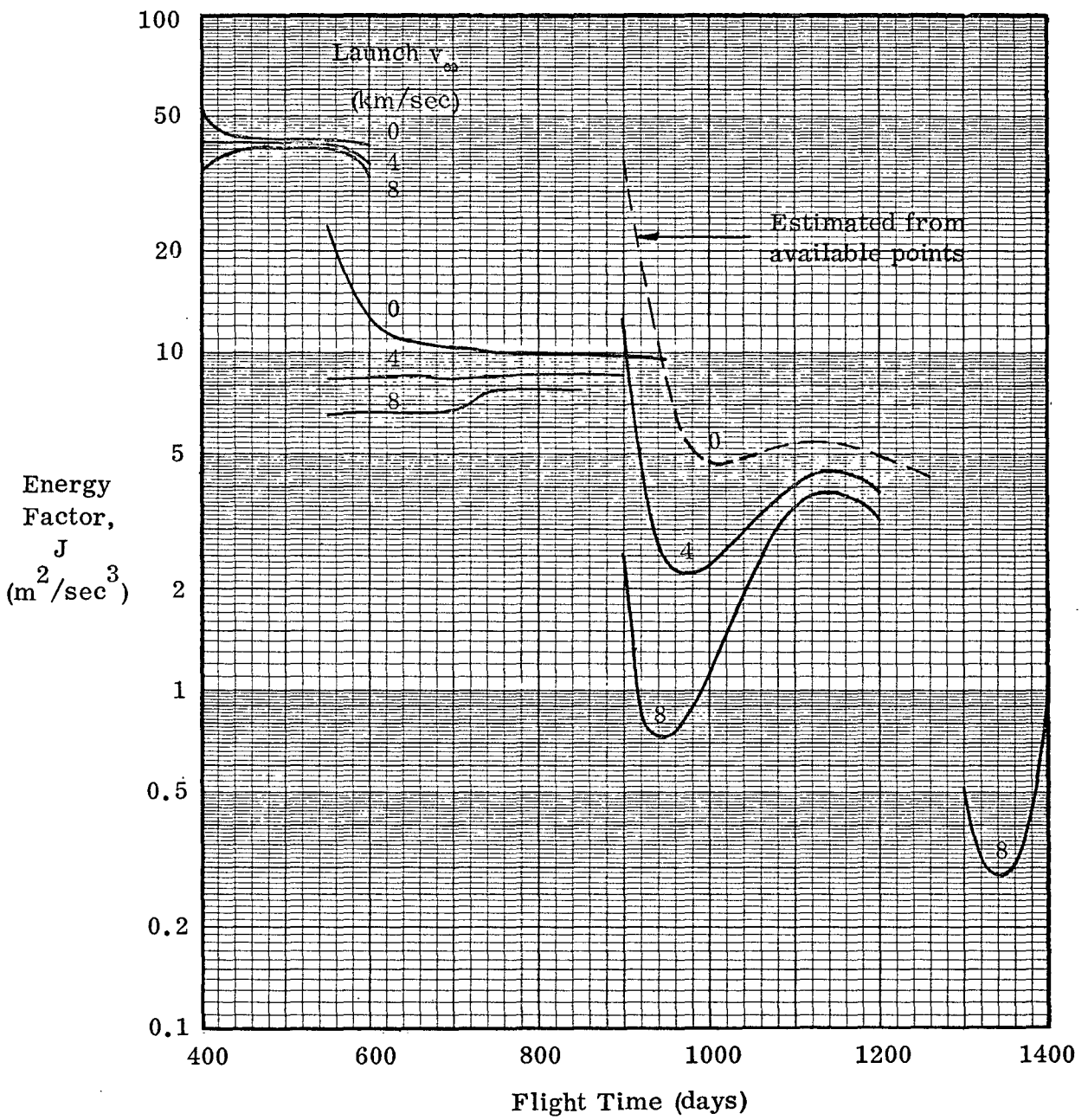

Figure 2 - Variation of energy factor with flight time.

1980 NEP ENCKE RENDEZVOUS MISSION

Arrival on October 17, 1980

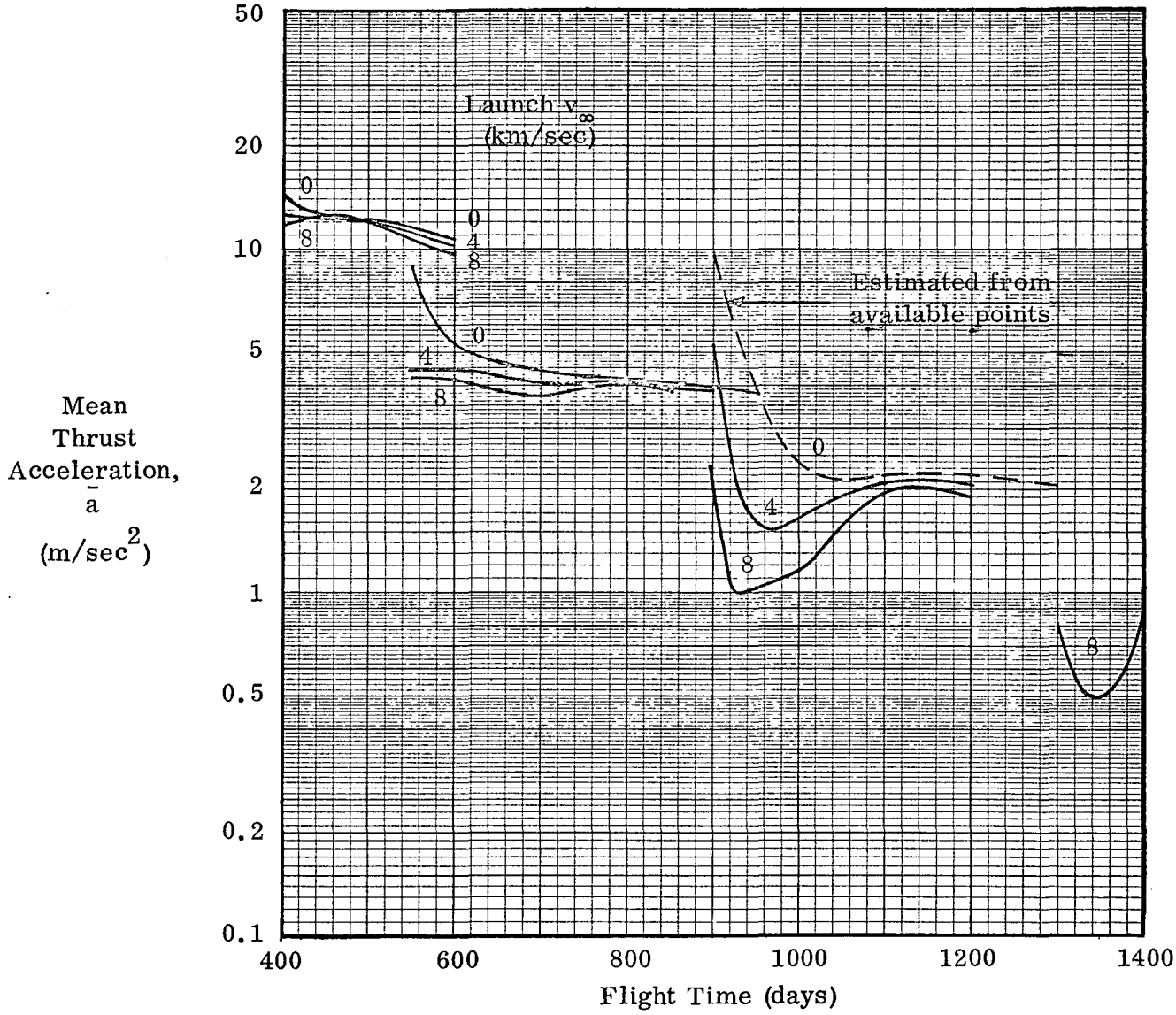

Figure 3 - Variation of mean thrust acceleration with flight time.

1980 NEP ENCKE RENDEZVOUS MISSION

Arrival on October 17, 1980

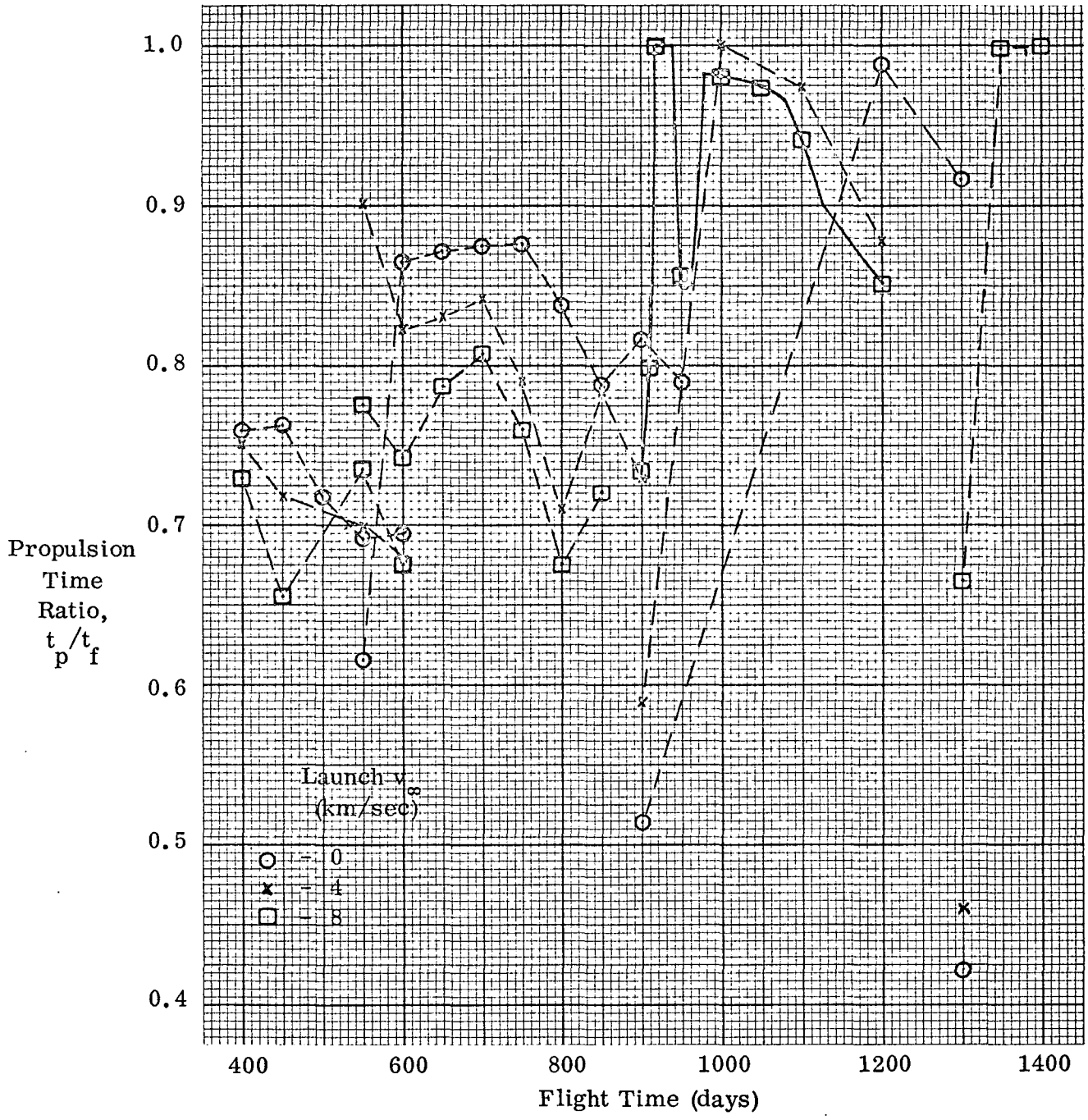

Figure 4 - Variation of propulsion time ratio with flight time.

1980 NEP ENCKE RENDEZVOUS MISSION

Arrival on October 17, 1980

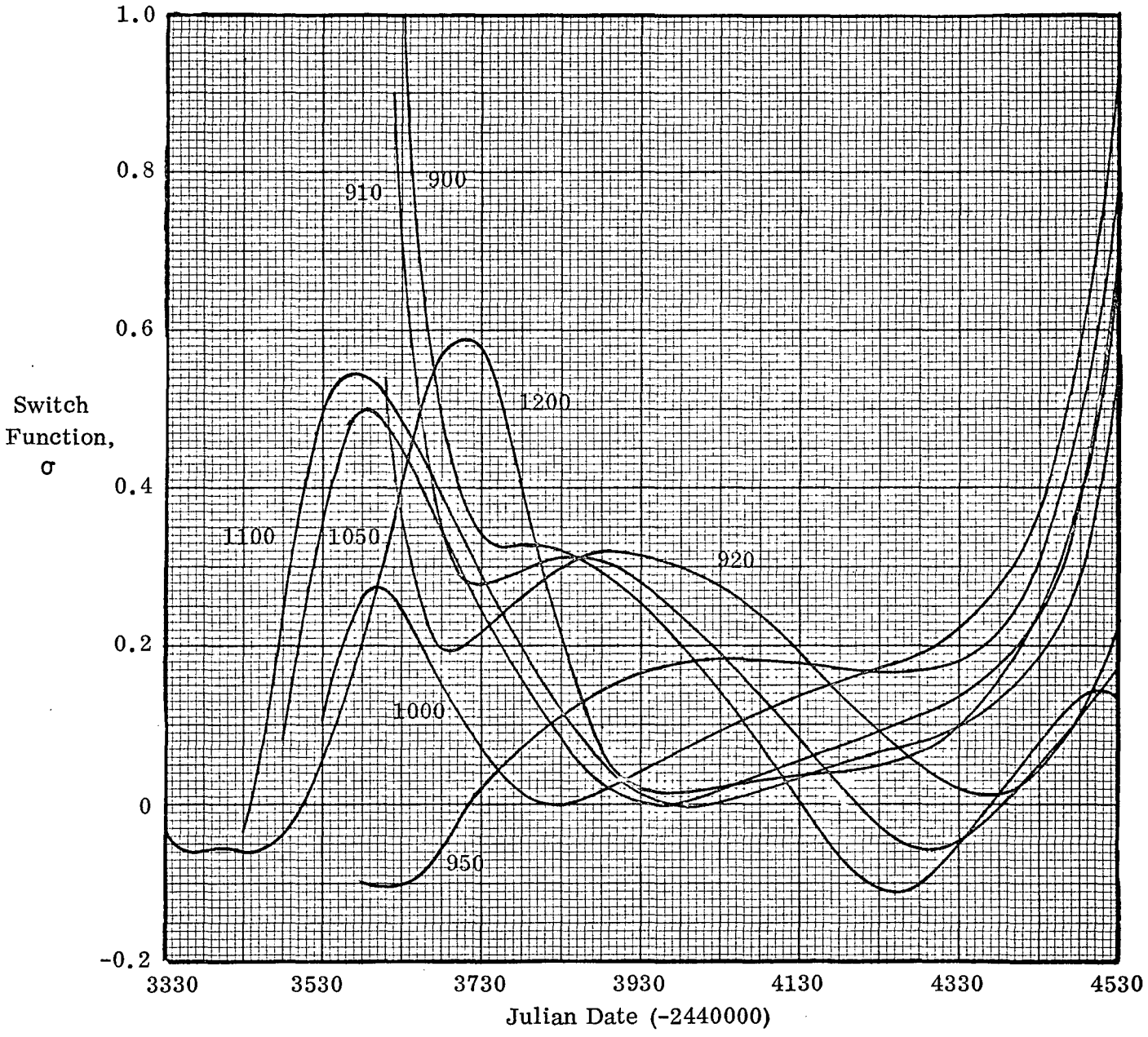

Figure 5 - NEP engine switch function time histories.

1980 NEP ENCKE RENDEZVOUS MISSION

Arrival on October 17, 1980

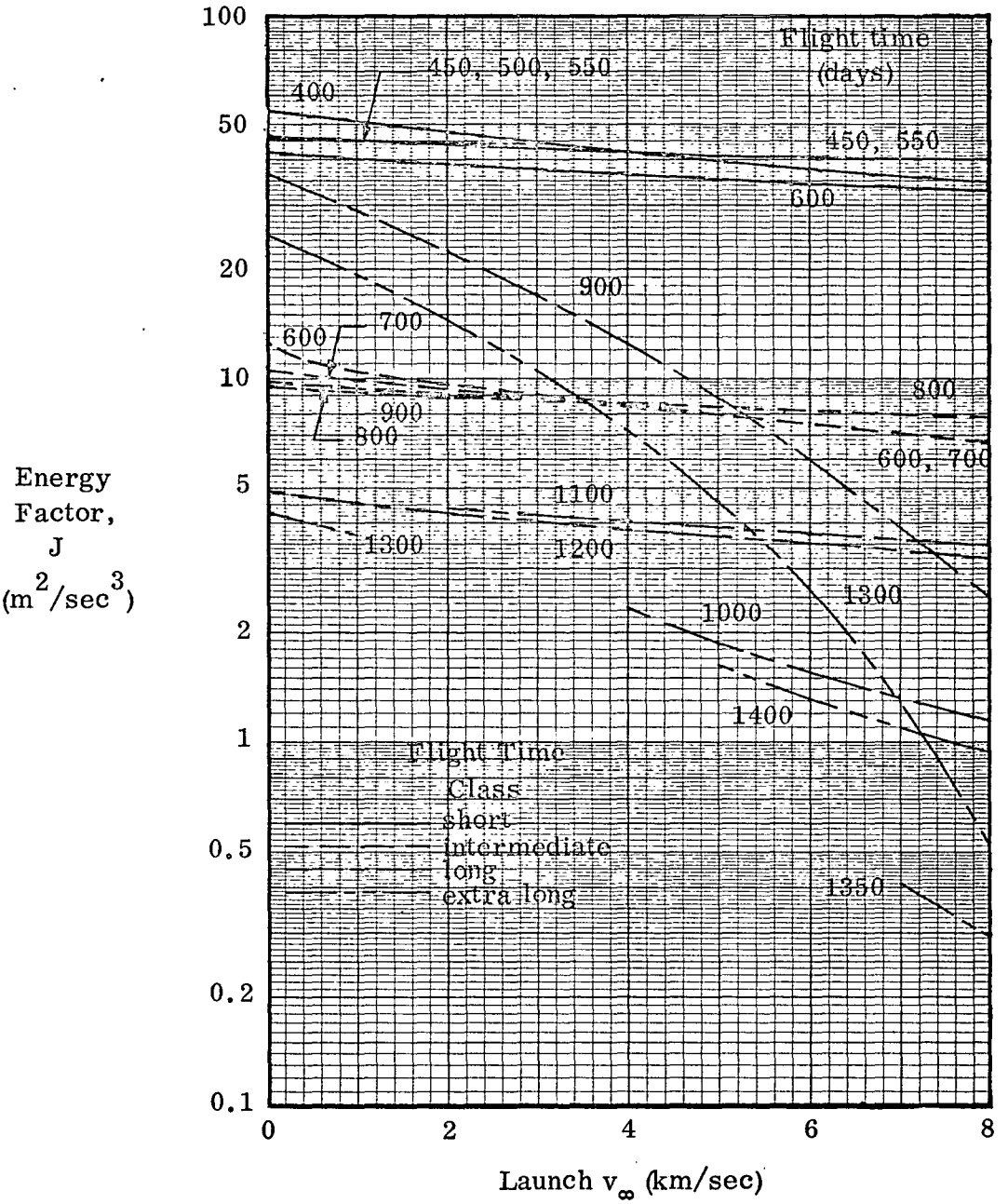

Figure 6- Variation of energy factor with launch excess speed.

1980 NEP ENCKE RENDEZVOUS MISSION

Arrival on October 17, 1980

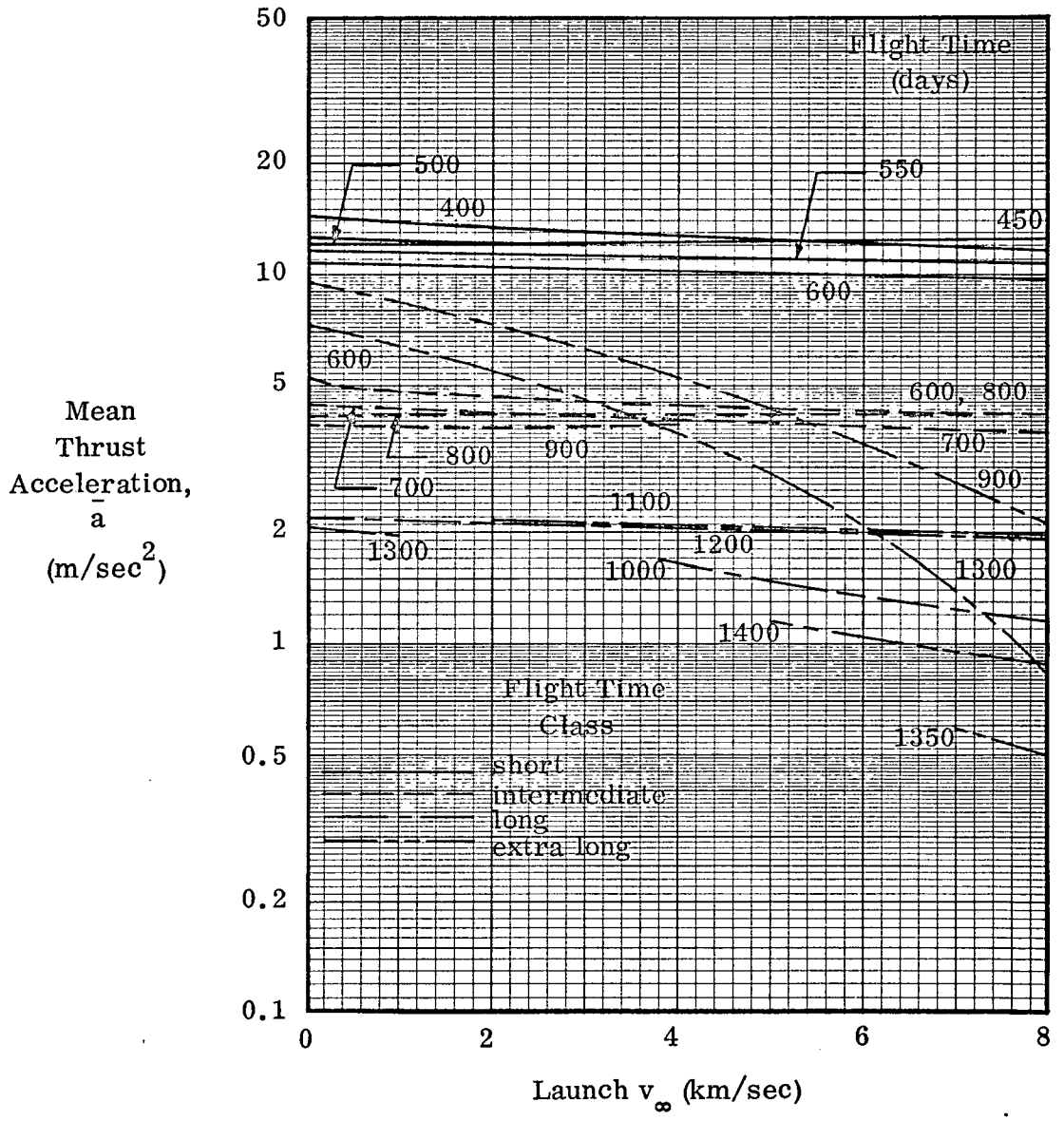

Figure 7 - Variation of mean thrust acceleration with launch excess speed.

1980 NEP ENCKE RENDEZVOUS MISSION

Arrival on October 17, 1980

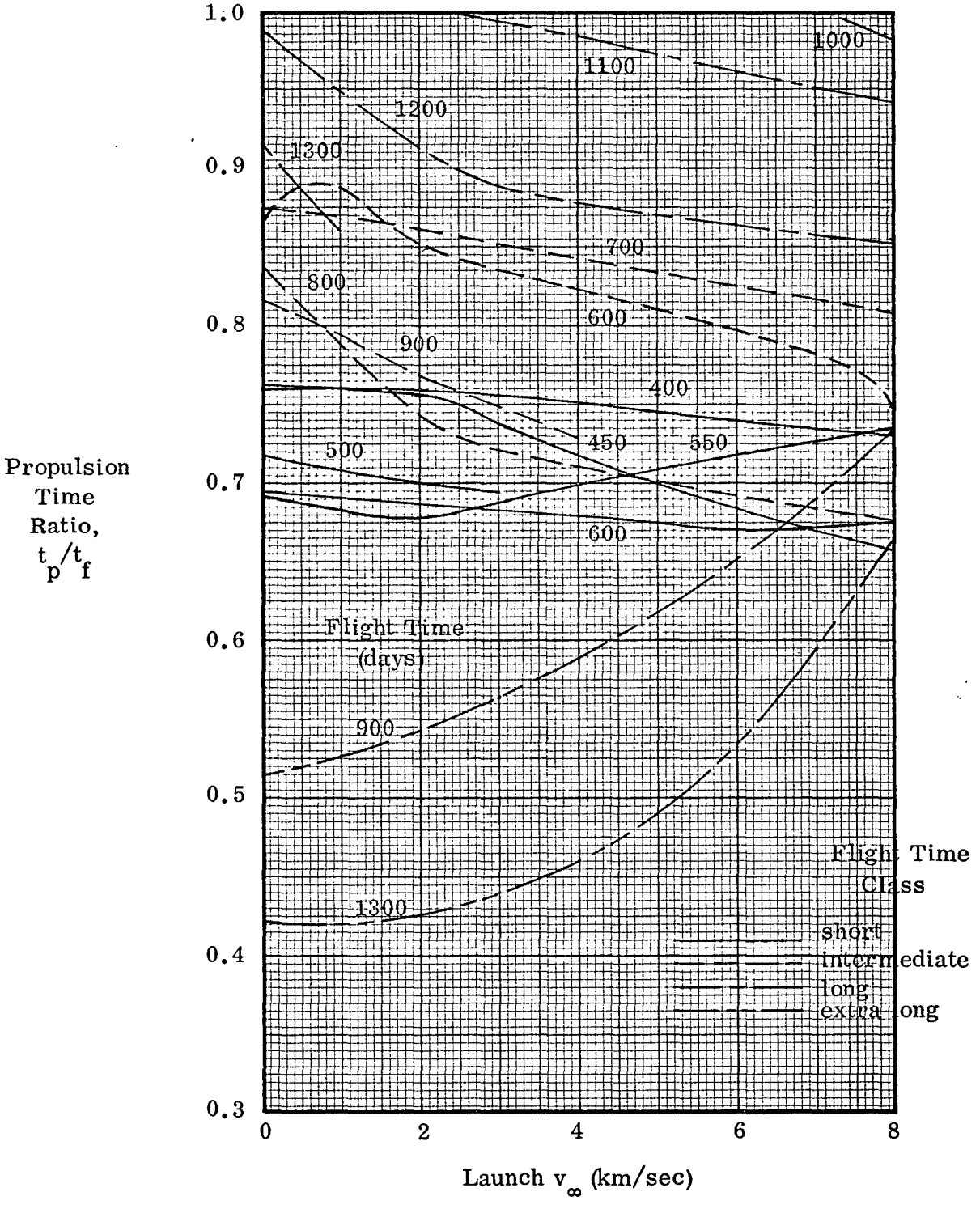

Figure 8 - Variation of propulsion time ratio with launch excess speed.

1980 NEP ENCKE RENDEZVOUS MISSION

Arrive on October 17, 1980

Intermediate Flight Time Class

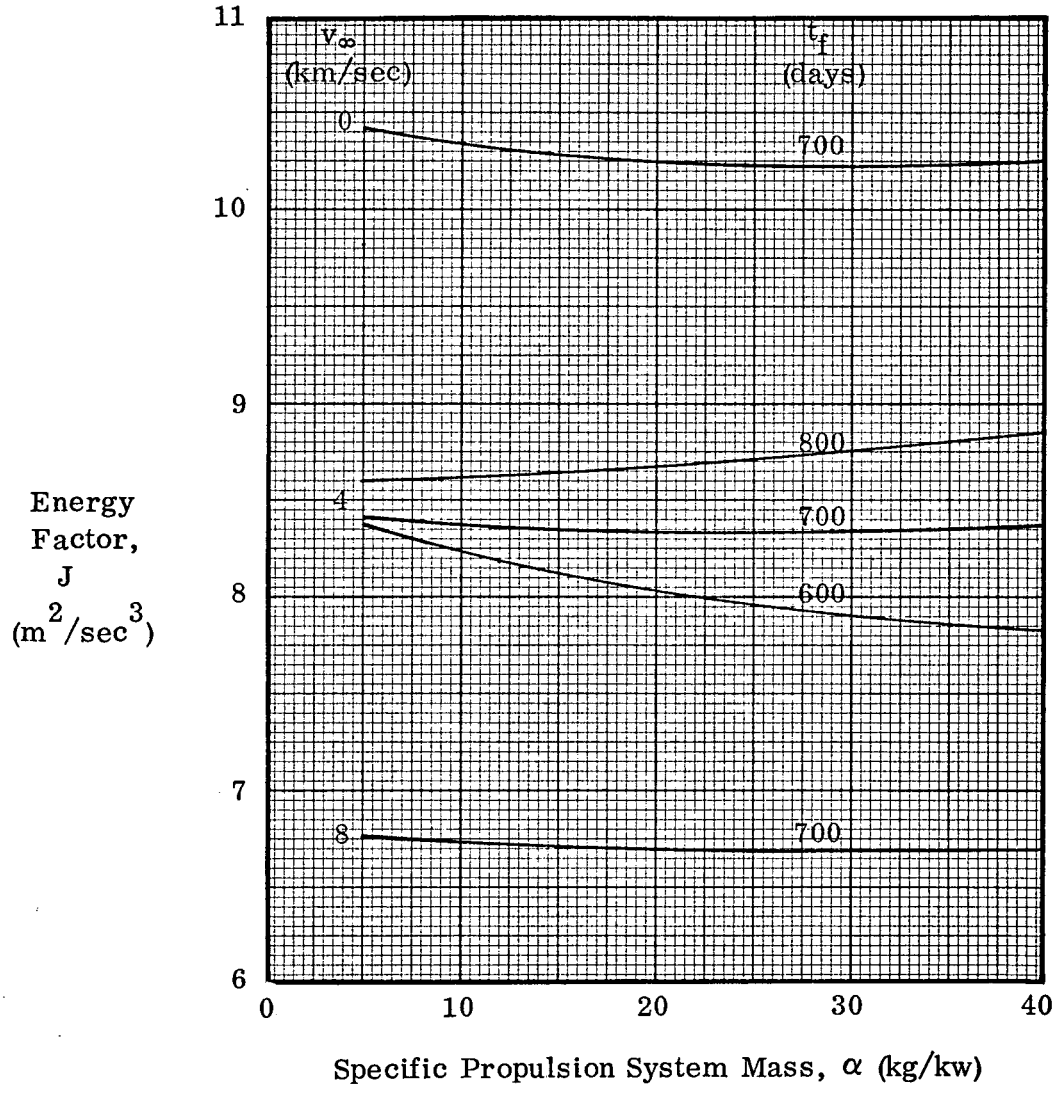

Figure 9 - Variation of energy factor with specific propulsion system mass.

1980 NEP ENCKE RENDEZVOUS MISSION

Arrival on October 17, 1980

Intermediate Flight Time Class

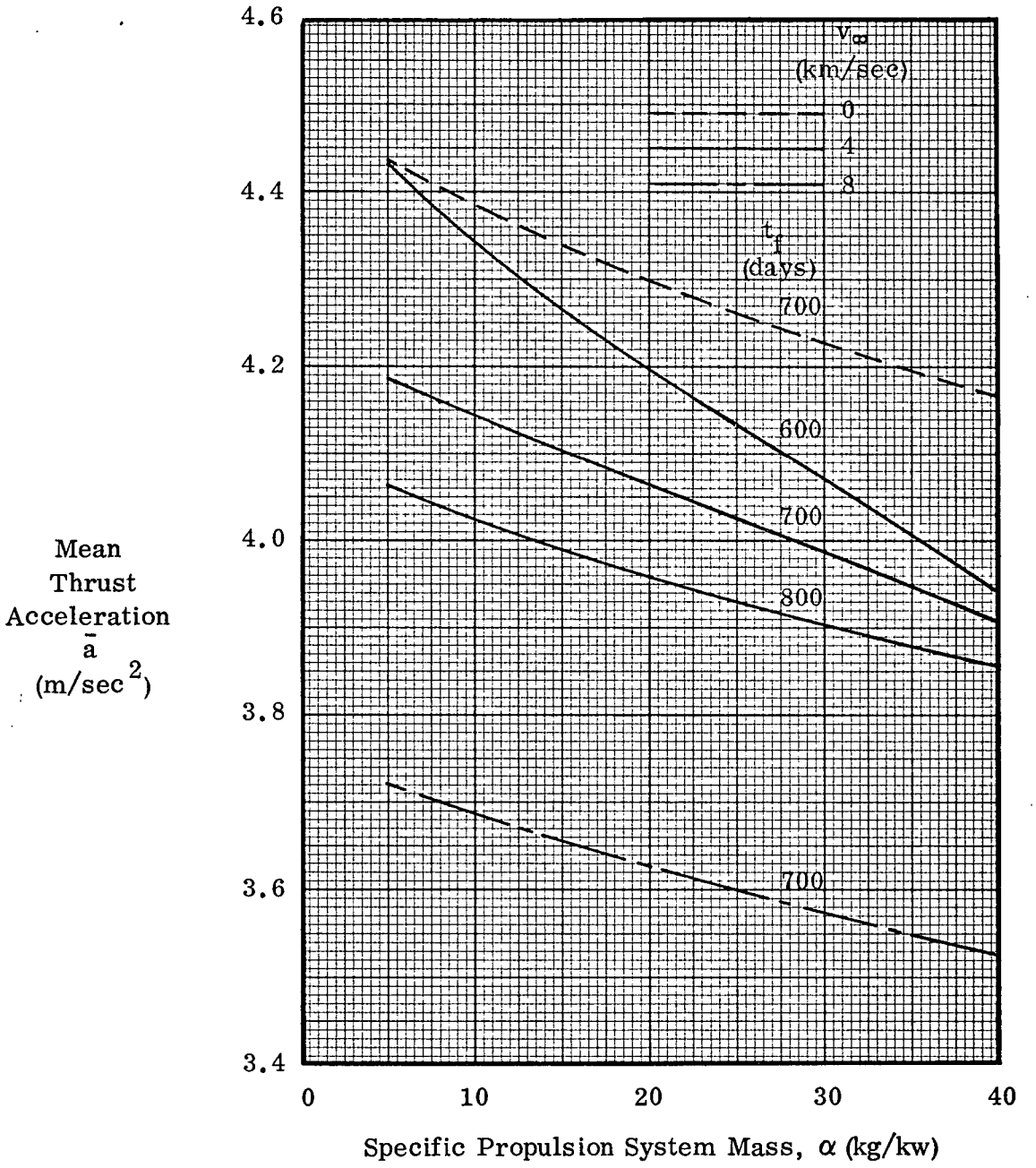

Figure 10 - Variation of mean thrust acceleration with specific propulsion system mass.

1980 NEP ENCKE RENDEZVOUS MISSION

Arrival on October 17, 1980

Intermediate Flight Time Class

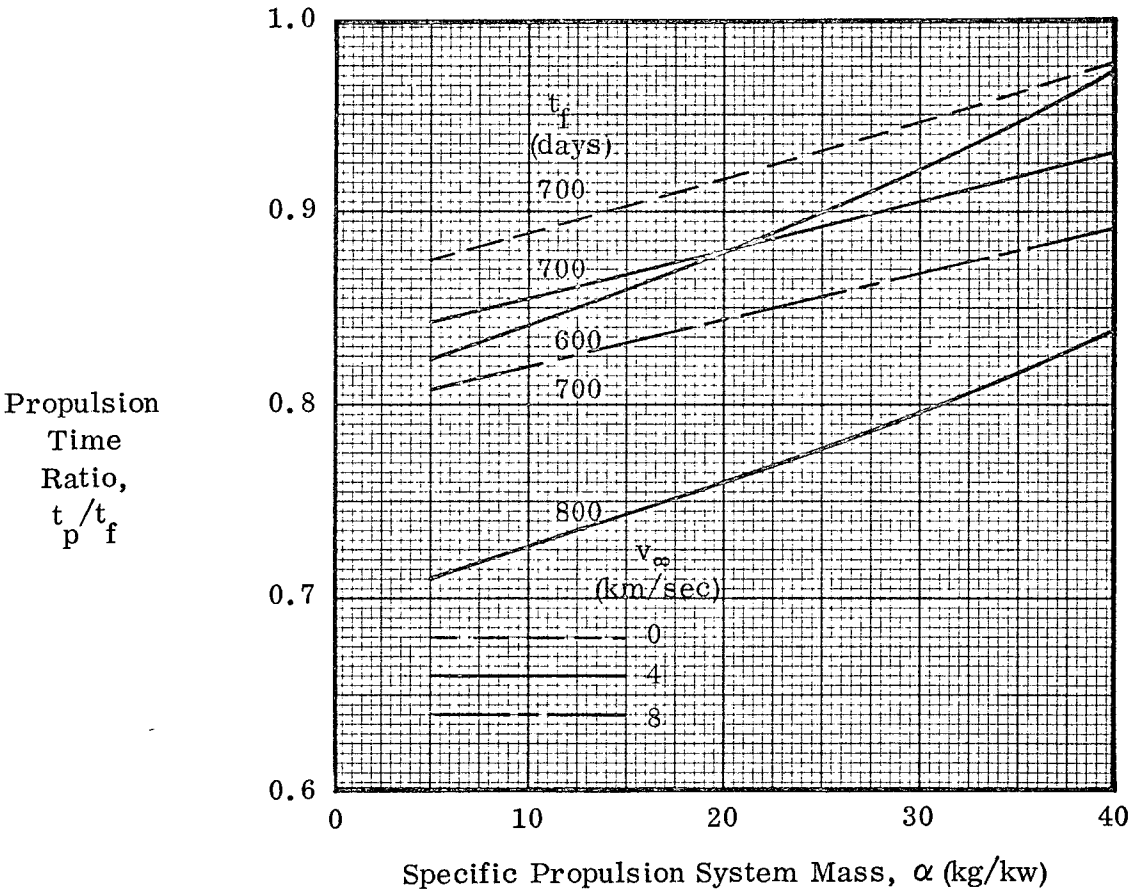

Figure 11 - Variation of propulsion time ratio with specific propulsion system mass.

1980 NEP ENCKE RENDEZVOUS MISSION

Specified t_o, t_f, m_o and v_∞'s

Optimized c

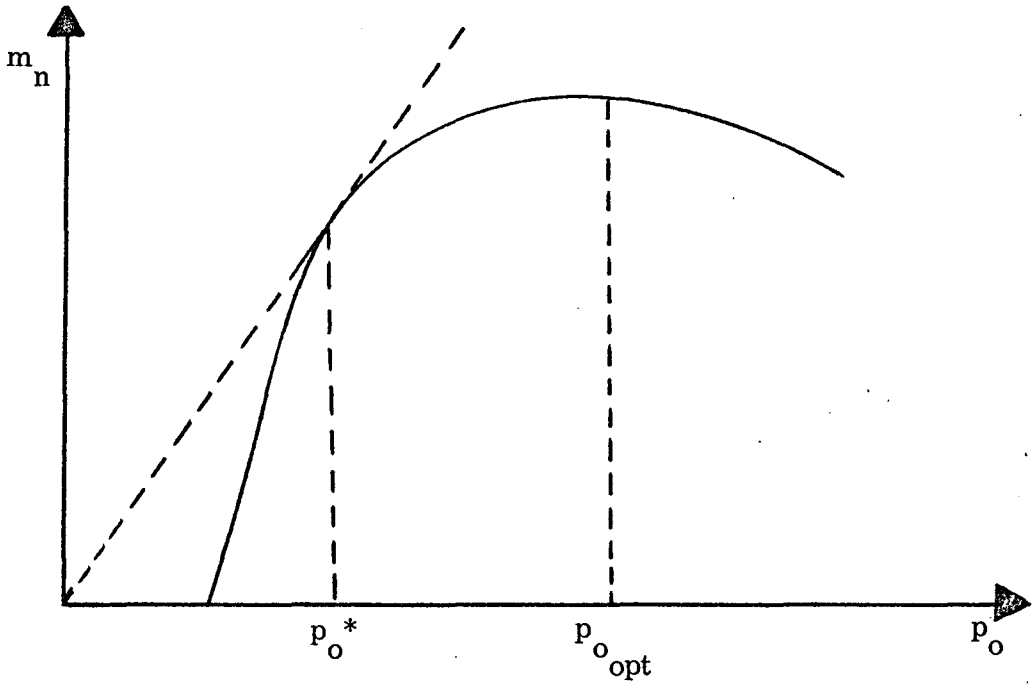

Figure 12 - Typical behavior of net spacecraft mass as a function of power level.

1980 NEP ENCKE RENDEZVOUS MISSION

700 Day Flight Time Arriving on October 17, 1980

Titan III D/Centaur Launch Vehicle

α = 5 kg/kw

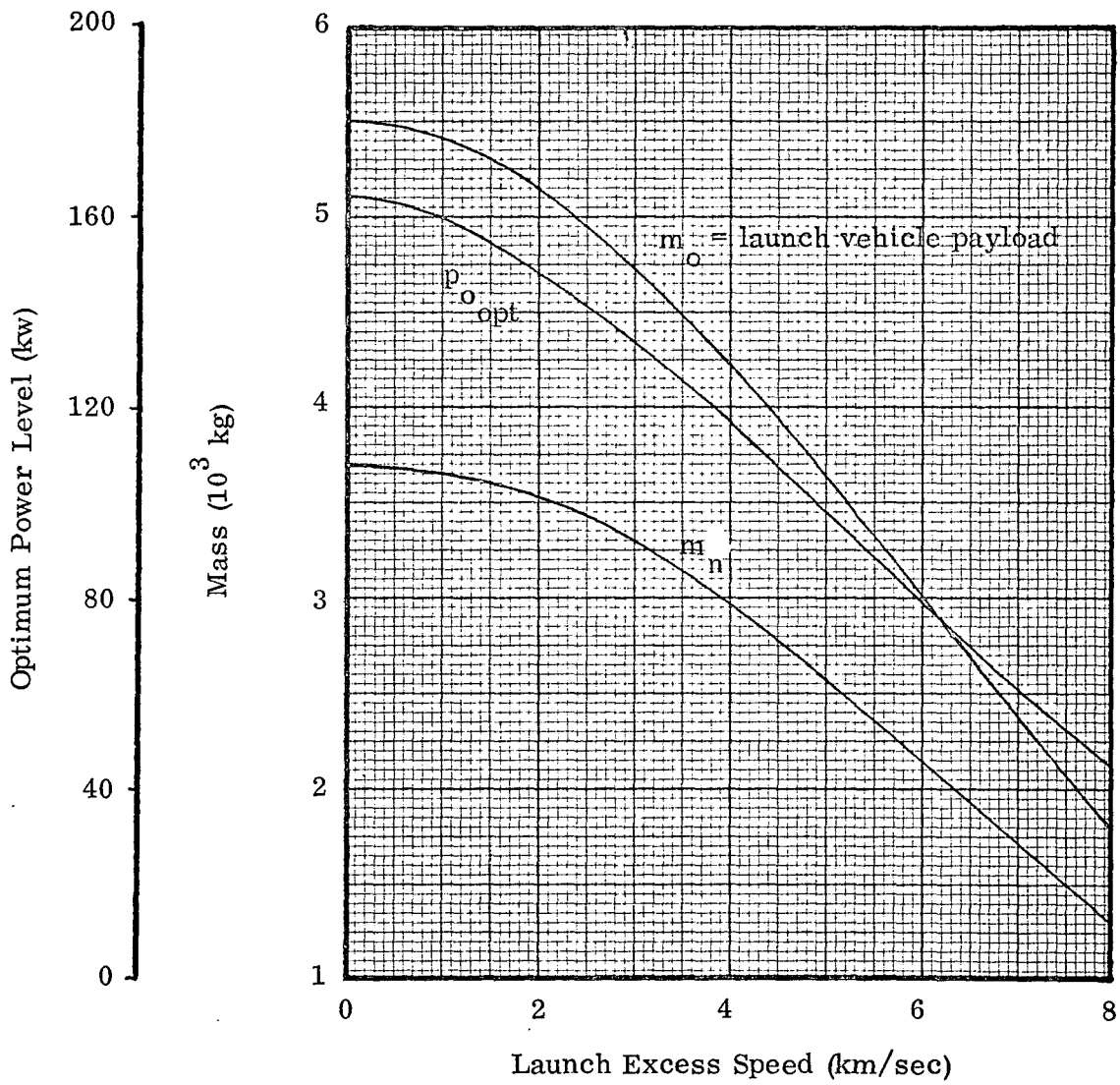

Figure 13 - Performance Parameters for Encke Mission at Optimum Power Level.

1980 NEP ENCKE RENDEZVOUS MISSION

700 Day Flight Time Arriving on October 17, 1980

Tital III D/Centaur Launch Vehicle

$\alpha = 5$ kg/kw

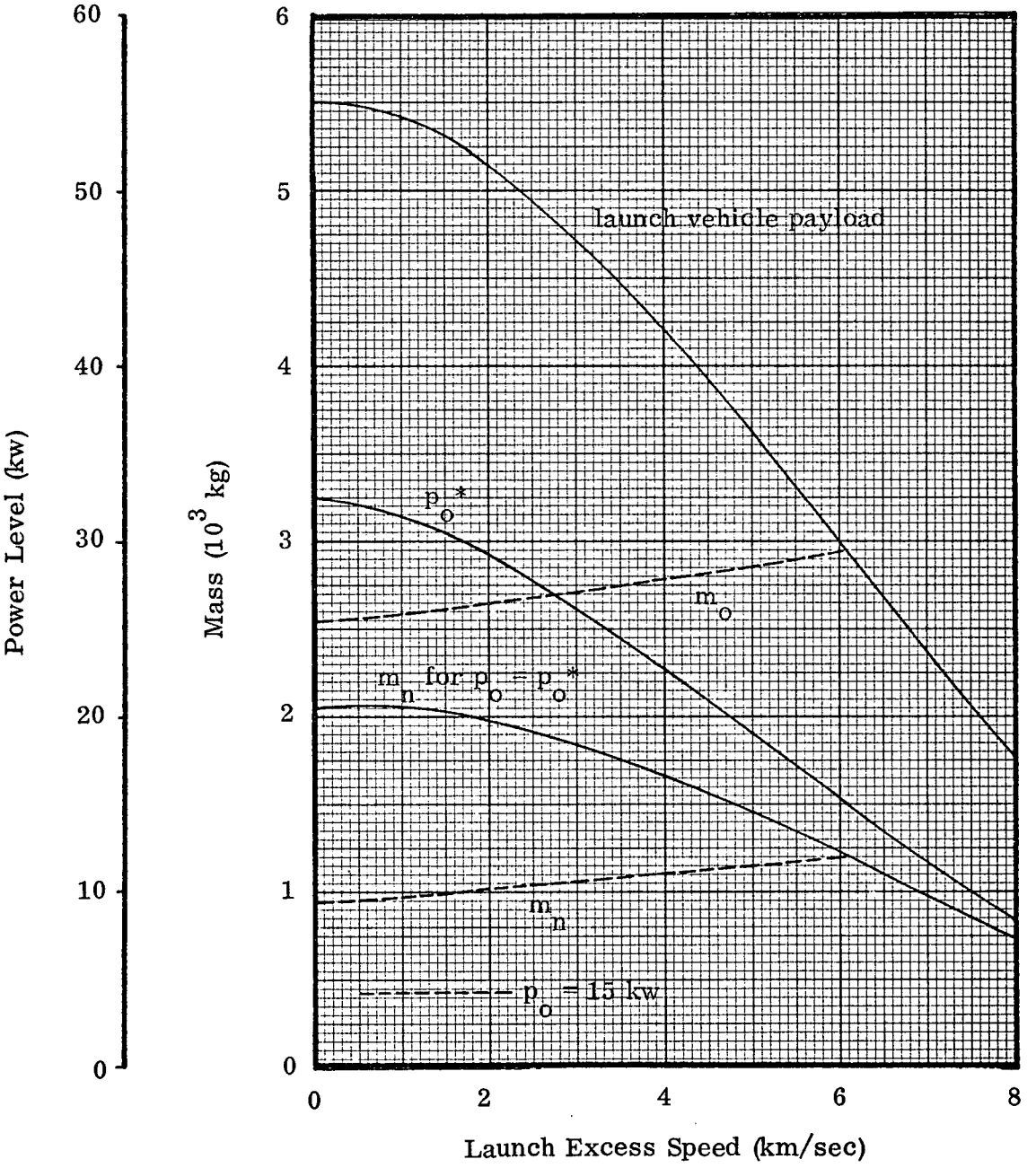

Figure 14 - Performance Parameters for Encke Mission at Constrained Power Levels using Multi-Parameter Independent Mode.